

# Proteus: Achieving High-Performance Processing-Using-DRAM via Dynamic Precision Bit-Serial Arithmetic

Geraldo F. Oliveira<sup>†</sup>    Mayank Kabra<sup>†</sup>    Yuxin Guo<sup>‡</sup>    Kangqi Chen<sup>†</sup>    A. Giray Yağlıkçı<sup>†</sup>  
Melina Soysal<sup>†</sup>    Mohammad Sadrosadati<sup>†</sup>    Joaquin Olivares Bueno<sup>\*</sup>  
Saugata Ghose<sup>∇</sup>    Juan Gómez-Luna<sup>§</sup>    Onur Mutlu<sup>†</sup>

<sup>†</sup> ETH Zürich    <sup>‡</sup> Cambridge University    <sup>\*</sup> Universidad de Córdoba  
<sup>∇</sup> Univ. of Illinois Urbana-Champaign    <sup>§</sup> NVIDIA Research

*Processing-using-DRAM (PUD) is a paradigm where the analog operational properties of DRAM structures are used to perform bulk logic operations. While PUD promises high throughput at low energy and area cost, we uncover three limitations of existing PUD approaches that lead to significant inefficiencies: (i) static data representation, i.e., 2's complement with fixed bit-precision, leading to unnecessary computation over useless (i.e., inconsequential) data; (ii) support for only throughput-oriented execution, where the high latency of individual PUD operations can only be hidden in the presence of bulk data-level parallelism; and (iii) high latency for high-precision (e.g., 32-bit) operations. To address these issues, we propose Proteus, which builds on two key ideas. First, Proteus parallelizes the execution of independent primitives in a PUD operation by leveraging DRAM's internal parallelism. Second, Proteus reduces the bit-precision for PUD operations by leveraging narrow values (i.e., values with many leading zeros). We compare Proteus to different state-of-the-art computing platforms (CPU, GPU, and the SIMDRAM PUD architecture) for twelve real-world applications. Using a single DRAM bank, Proteus provides (i) 17×, 7.3×, and 10.2× the performance per mm<sup>2</sup>; and (ii) 90.3×, 21×, and 8.1× lower energy consumption than that of the CPU, GPU, and SIMDRAM, respectively, on average across twelve real-world applications. Proteus incurs low area cost on top of a DRAM chip (1.6%) and CPU die (0.03%).*

## 1. Introduction

Processing-in-memory (PIM) [1–12] aims to alleviate the ever-growing cost of moving data between computing (e.g., CPU, GPU) and memory (e.g., DRAM) elements. In PIM architectures, computation is done by adding logic near memory arrays, i.e., processing-near-memory (PNM) [13–98], or by using the analog properties of the memory arrays, i.e., processing-using-memory (PUM) [66, 99–139]). Many prior works [66, 101–107, 110, 114–117, 119, 120, 126, 129, 130, 132, 133, 140, 141] demonstrate the feasibility of processing-using-DRAM (PUD), which use DRAM cells to implement in-DRAM row copy [104, 110, 116], Boolean [101, 103, 107], and arithmetic [106, 132, 133, 141–143] operations. PUD systems often employ a *bulk bit-serial* execution model, where each Boolean primitive operates across entire DRAM rows, with each row containing one bit from many input operands. The predefined sequence of DRAM commands used to implement each operation are stored in a *μProgram*.

In this work, we uncover three limitations that significantly hurt the performance and efficiency of PUD architectures. First, they employ a *static bit-precision* for operands (i.e., the number of bits used to represent an operand), which is wider than the maximum data values being computed on. This results in significant wasted latency and energy to perform calculations on inconsequential bits (e.g., leading zeros in case of positive numbers or leading ones in case of negative numbers). Second, they aim to *maximize execution throughput* for large data sets, to overcome long bit-serial latencies and take advantage of the large amount of in-DRAM parallelism. Whenever these architectures execute on smaller data sets, much of this parallelism is not fully utilized, *even though there are opportunities to better exploit this parallelism to improve latency and efficiency*. Third, they suffer from *high latencies for high-precision computation* due to their bit serialization. Ultimately, these limitations exist because there is no one-size-fits-all solution for data representation and execution model across a wide range of applications.

Our goal in this work is to overcome the three limitations of PUD architectures caused by naively employing a bit-serial execution model. To this end, we propose *Proteus*,<sup>1</sup> an efficient PUD framework with adaptive bit-precision and dynamic arithmetic. The *key ideas* behind *Proteus* are: (i) fully leverage the parallelism within a DRAM bank to accelerate the execution of various bit-serial and bit-parallel arithmetic operations, and (ii) decide at runtime the best-performing bit-precision, data representation format, and algorithmic implementation of each PUD operation. *Proteus* is composed of three main components: *parallelism-aware μProgram library*, *dynamic bit-precision engine*, and *μProgram select unit*.

First, we build a *parallelism-aware μProgram library*, which consists of hand-tuned implementations of key arithmetic operations using various bit-serial and bit-parallel algorithms and data representation formats. To improve their performance, we carefully craft different implementations of a given PUD operation to parallelize the execution of independent steps in a *μProgram* across different DRAM subarrays. Our *parallelism-aware μProgram library* considers different data representation formats that can be more suitable for high-precision arithmetic.

<sup>1</sup>*Proteus* is a shape-shifting, prophetic sea god from Greek mythology, known for his ability to elude capture by changing forms. As such, *Proteus* changes the bit-precision of PUD operations to improve performance.

metic. Namely, we implement variations of our algorithms using both 2’s complement and redundant binary representation (RBR) [144–146]. Unlike binary numeral systems, RBR uses a pair of bits to represent an operand. This allows RBR-based arithmetic to be performed *without* the need for long and costly carry propagation chains. In the end, the *parallelism-aware  $\mu$ Program library* contains a collection of possible implementations of desired PUD operations, each of which with different time complexities that depend on the target bit-precision. Second, we devise a new *dynamic bit-precision engine* to identify the appropriate initial bit-precision for a given PUD operation. We implement the *dynamic bit-precision engine* by augmenting prior works’ data transposition engine [141, 142]. Before PUD execution, the data transposition engine captures and transposes (from the standard horizontal data layout to the PUD vertical data layout) cache lines that are about to be evicted from the last-level cache (LLC) to DRAM and belong to a previously-identified PUD memory object. During this process, our *dynamic bit-precision engine scans* the content of the evicted cache line to identify the largest value belonging to a PUD memory object. Third, when the user issues a PUD operation, the  *$\mu$ Program select unit* probes the *dynamic bit-precision engine* to identify the most suitable bit-precision for the PUD operation and selects the best performing  $\mu$ Program from the *parallelism-aware  $\mu$ Program library*.

We compare the benefits of *Proteus* to different state-of-the-art computing platforms (CPU, GPU, and the SIMDRAM [142] PUD mechanism). We comprehensively evaluate *Proteus*’s performance for twelve real-world applications. Using a single DRAM bank, *Proteus* provides (i) 17 $\times$ , 7.3 $\times$ , and 10.2 $\times$  the performance per mm<sup>2</sup>; and (ii) 90.3 $\times$ , 21 $\times$ , and 8.1 $\times$  lower energy consumption than that the CPU, GPU, and SIMDRAM, respectively, on average across all twelve real-world applications. *Proteus* incurs low area cost on top of a DRAM chip (1.6%) and CPU die (0.03%).

We make the following key contributions:

- To our knowledge, this is the first framework to enable PUD operations with dynamic bit-precision, adaptive data representation, and flexible arithmetic.
- *Proteus* provides a three-component framework to transparently (i) identify the bit-precision for a PUD operation and (ii) select the best-performing implementation of the target PUD operation based on the target bit-precision.
- We extensively evaluate *Proteus* for twelve real-world applications, showing that *Proteus* outperforms state-of-the-art PUD framework and processor-centric design while incurring low area cost to the system.

## 2. Background

We first briefly explain the architecture of a typical DRAM chip. Next, we describe prior DRAM enhancements and PUD works that *Proteus* builds on top of.

### 2.1. DRAM Organization & Operation

**DRAM Organization.** Fig. 1 shows the hierarchy of a DRAM system. A *DRAM module* (Fig. 1a) has several (e.g., 8–16)

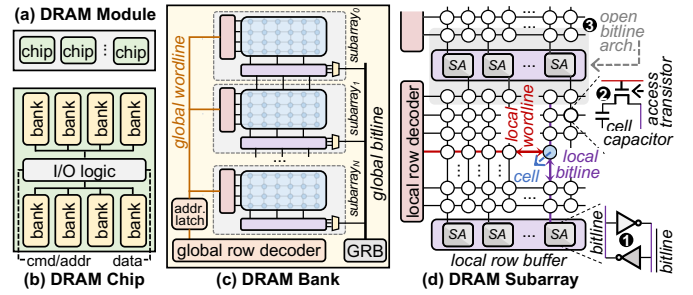


Figure 1: DRAM organization. Adapted from [120].

DRAM chips. A *DRAM chip* (Fig. 1b) has multiple banks (e.g., 8–16). A *DRAM bank* (Fig. 1c) has (i) multiple (e.g., 64–128) 2D arrays of DRAM cells known as *DRAM subarrays*; (ii) a *global row decoder* and a *global address latch* that select a row of cells in a subarray through *global wordlines*; (iii) *column select logic* (CSL) that selects portions (e.g., 64-bit) of the row; and (iv) a *global row buffer* (GRB) that transfers the selected fraction of the data from the row through *global bitlines*. Each subarray (Fig. 1d) contains (i) multiple rows (e.g., 512–1024) and columns (e.g., 2–8 kB [147–149]) of DRAM cells, (ii) a *local row decoder* that activates a *local wordline*, and (iii) a *local row buffer* containing a row of *sense amplifiers* (SAs; ❶ in Fig. 1d) to latch data from an activated row. A DRAM cell (❷) consists of an *access capacitor*, which connects a transistor that stores the data value with a *local bitline* shared by all cells in the same column. Modern DRAM employs an *open bitline architecture* [150, 151], fitting only enough SAs in one local row buffer to latch half a row of cells. To latch the entire row, a subarray connects to *two* local row buffers, one above the cell array and one below (❸).

**DRAM Operation.** The memory controller issues three commands to service a DRAM request. Initially, the local bitlines are set at a reference voltage. The first command, *ACTIVATE* (ACT), connects DRAM cells in a row to its local bitline, and the cell’s transistor shares its charge with the bitline to shift the bitline voltage higher (or lower) if the cell stores a ‘1’ (‘0’). The local row buffer amplifies the shifts to CMOS-readable values (simultaneously restoring charge to the DRAM cell). The latency from the start of activation until charge restoration is called  $t_{RAS}$ . The second command, *READ* (RD), returns a cache line of data from the local row buffer. The third command, *PRECHARGE* (PRE), disconnects DRAM cells from the bitlines, and returns the bitlines to their reference voltage. The precharge latency is called  $t_{RP}$ .

### 2.2. Processing-Using-DRAM

**In-DRAM Row Copy.** RowClone [104] enables copying a row *A* to a row *B* in the *same* subarray by issuing two consecutive ACT commands to these two rows, followed by a PRE command. This command sequence is called AAP. LISA [152] expands RowClone functionally to enable the execution of in-DRAM row copy operations across DRAM rows in *different* subarrays of a DRAM chip by connecting local row buffers of neighbor subarrays using isolation transistors.

**In-DRAM Bitwise Operations.** Ambit [101] shows that a simultaneous *triple row activation (TRA)* can perform *in-DRAM* bitwise AND/OR operations. Ambit implements TRA using a custom row decoder, and introduces a new command called AP that issues a TRA followed by a PRE. SIMDRAM [142] builds on top of Ambit to implement and expose high-level in-DRAM operations ( $\mu$ Programs). A  $\mu$ Program consists of a sequence of AAPs (row copies) and APs that are generated offline, and exposed to the programmer as *bbop* instructions. To implement carry propagation, SIMDRAM employs a *vertical* data layout, where all bits of a data word are stored in a single DRAM column (or bitline), and executes bit-serially. Such execution model allows SIMDRAM to perform *implicit bit-shift* operations via in-DRAM row copies, e.g., SIMDRAM performs a left-shift-by-one operation by copying the data in DRAM row  $j$  to DRAM row  $j + 1$ .

### 3. Motivation

In this section, we discuss the three limitations of prior PUD architectures: *static data representation*, *support for only throughput-oriented execution*, and *high latency for high-precision operands*.

**Static Data Representation.** PUD architectures naively utilized conventional data formats (e.g., 2’s complement) and fixed operand bit-precision (e.g., 32-bit integers) to implement bit-serial computation. However, because bit-serial latency scales with the bit-precision, these architectures experience subpar performance since application’s data with small dynamic range (i.e., narrow values) are often stored in large data formats [153–160] that waste most of the bit-precision. Note that, most often, the data values become narrow dynamically at runtime. Narrow values have been exploited in many scenarios, e.g., cache compression [153–155, 160], register files [158, 161–163], logic synthesis [164–166].

**Opportunity 1: Narrow Values for PUD Computation.** Narrow values can be exploited to reduce the bit-precision of a PUD operation to that of the best-fitting number of bits; thus, improving overall performance. We quantify the required bit-precision in PUD-friendly real-world applications in Fig. 2. We define as *required bit-precision* the minimum number of bits required to represent the input operands of the PUD operation.<sup>2</sup> We collect the required bit-precision dynamically in three main steps: we (i) instrument loops in applications that can be auto-vectorized using LLVM’s loop auto-vectorization pass [167–170] (since prior work [141] shows that such loops are suitable for PUD execution) to output the data such loop consumes, (ii) execute the application to completion, (iii) post-process the output file containing the loop information data to calculate the required bit-precision. We make two observations. First, all our real-world applications display a *significant* amount of narrow values. In such applications, the input bit-precision can be reduced from the native 32-bit to 20-bit (min.

<sup>2</sup>For example, if the input operand is an integer storing the value ‘2’, the required bit-precision for such an input operand would be 3 bits (two bits to represent the data, and one bit to represent the sign value).

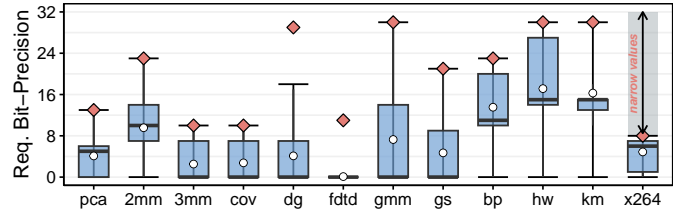


**Figure 2: Bit-precision distribution for 12 applications. The box represents the 25th to 75th percentiles, with whiskers extending to the smallest/largest precision (with a diamond at the largest precision and a bubble at the mean precision).**

of 8-bit, max. of 30-bit) on average across *all* applications. By doing so, the performance of the underlying PUD architecture can improve by 1.6 $\times$ , in case the application utilizes linearly-scaling PUD operations (such as addition), or 2.6 $\times$ , in case the application utilizes quadratically-scaling PUD operations (such as multiplication). Second, the bit-precision significantly varies for a given application. This indicates the need for a mechanism that can *dynamically* identify the target bit-precision for a given PUD operation (similar to prior works that leverage narrow values for tasks other than PUD [153–162, 171, 172]). As prior work points out [157], static compiler analyses *cannot* identify the bit-precision of dynamically allocated and initialized data arrays. We investigated several prior compiler works [164, 173–176] that perform bit-width identification for different reasons, e.g., to reduce the size of registers generated by high-level synthesis tools. However, such works are limited to identifying the bit-precision of statically allocated variables.

**Throughput-Oriented Execution.** PUD architectures favor throughput-oriented execution as DRAM parallelism can partially hide the latency of consecutive activations in a  $\mu$ Program. To further improve throughput, prior works [142, 143] use DRAM’s bank-level parallelism (BLP) to (i) distribute independent  $\mu$ Programs across multiple DRAM banks [142], or (ii) parallelize data writing and PUD computation of *different*  $\mu$ Programs targeting *different* banks [143]. However, such approaches fail to reduce the latency of a *single*  $\mu$ Program.

**Opportunity 2: DRAM Parallelism for Latency-Oriented Execution.** We make the *key observation* that several primitives in a  $\mu$ Program can be executed concurrently, as they are independent of one another. Fig. 3 shows this opportunity for a two-bit addition, and how we could concurrently execute primitives for the addition if its operands were distributed across two different subarrays, since the only dependency between the two bits of the addition is the *carry propagation* (① in Fig. 3a). By placing each bit of the operand into a different subarray, we can parallelize independent primitives and serialize *only* for the carry propagation (② in Fig. 3b).

**High-Precision Computation.** For operations that require high bit-precision, PUD architectures suffer from high latency. For example, even when employing multiple (i.e., 16) parallel DRAM banks, SIMDRAM’s throughput for 32-bit and 64-bit division is 0.8 $\times$  and 0.5 $\times$  that of a 16-core CPU system [142]. This is because the latency of bit-serial multiplication and division scales *quadratically* with the bit-precision.

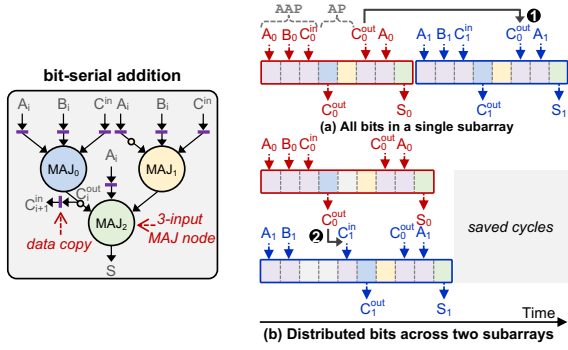


Figure 3: Bit-serial addition graph (left); Time diagram for bit-serial addition with one (a) and two (b) subarrays (right).

**Opportunity 3: Alternative Data Representation for High Precision Computation.** The high latency associated with high-precision computation is an *inherent* property of coupling the binary numeral system with bit-serial computation. Thus, we investigate an alternative data representation, i.e. the *redundant binary representation (RBR)* [144–146, 177, 178], for high-precision computation. RBR is a positional number system where each place  $i$ , which encodes  $2^i$ , is represented by two bits that can take on a value  $v \in \{-1, 0, 1\}$ , such that the magnitude of place  $i$  is  $v \times 2^i$ . For example, the 4-place number  $\langle 0, 1, 0, -1 \rangle$  represents  $2^2 - 2^0 = 3$ . PUD execution can take advantage of two properties of RBR-based arithmetic: (i) the operations no longer need to propagate carry bits through the full width of the data (e.g., RBR-based addition limits carry propagation to *at most* two places [179]), and (ii) the operation latency is *independent* of the bit-precision.

**Goal.** Our goal in this work is to mitigate the three limitations of PUD architectures caused by naively employing a bit-serial execution model. To do so, we aim to *fully* exploit the opportunities that DRAM’s internal parallelism and dynamic bit-precision can provide to improve the latency of PUD operations, using different execution models (bit-serial and bit-parallel) and data-representation formats.

## 4. Proteus Overview

*Proteus* is a PUD framework with adaptive data precision and dynamic arithmetic. The *key ideas* behind *Proteus* are: (i) to leverage parallelism inside a subarray to accelerate PUD operations and (ii) to decide at runtime the best-performing bit-precision, data representation, and  $\mu$ Program implementation.

Fig. 4 provides a high-level overview of *Proteus*’s framework, its main components, and execution flow. *Proteus* is composed of three main components: *parallelism-aware  $\mu$ Program library*, *dynamic bit-precision engine*, and  *$\mu$ Program select unit*. These components are implemented in hardware alongside DRAM’s memory controller. The *parallelism-aware  $\mu$ Program library* and  *$\mu$ Program select unit* are part of *Proteus control unit*.

### 4.1. Main Components of Proteus

**Parallelism-Aware  $\mu$ Program Library.** *Proteus* incorporates a *parallelism-aware  $\mu$ Program library* (① in Fig. 4) that consists of (i) hand-optimized implementations of different  $\mu$ Programs

for key PUD operations (each with different performance and bit-precision trade-offs), and (ii) *cost model logic*. For each operation, we implement multiple  $\mu$ Programs (§5.2.2) that use different (i) bit-serial or bit parallel algorithms and (ii) data representation formats (i.e., 2’s complement or RBR). Each  $\mu$ Program uses a novel data mapping that enables the *concurrent* execution of multiple independent primitives across bits (§5.2.1). The performance of each  $\mu$ Program depends on the bit-precision, and the *cost model logic* selects the best-performing  $\mu$ Program for a given operation and target bit-precision. The *cost model logic* comprises of *pre-loaded cost-model lookup tables (LUTs)*, which list the most-suitable  $\mu$ Program for each bit-precision, and *select logic* to identify the target LUT for a *bbop* instruction. We use a Pareto analysis to populate the LUTs.

**Dynamic Bit-Precision Engine.** *Proteus*’s *dynamic bit-precision engine* (② in Fig. 4) aims to identify the dynamic range of *memory objects* associated with a PUD operation. To do so, we dynamically identify the *largest* input operand a PUD’s memory object stores. In state-of-the-art PUD architectures [110, 131, 132, 142, 143], cache lines belonging to a PUD’s memory object need to be transposed from the traditional horizontal data layout to a vertical data layout *prior* to the execution of a PUD operation. To efficiently perform such data transformation, SIMDRAM [142] implements a *data transposition unit*, which hides the data transposition latency by overlapping cache line evictions and data layout transformation. The data transposition engine consists of an *object tracker* table (a small cache that keeps track of memory objects that are used by PUD operations) and *data transpose engines*. The user/compiler informs the *object tracker* of PUD’s memory objects (both inputs and outputs) using a specialized instruction called *bbop\_trsp\_init*. *Proteus* leverages such data transposition unit to identify the largest value in a PUD’s memory object by adding: (i) a new field in the data transposition unit called *maximum value*, which stores the largest value in a given memory object; and (ii) a *dynamic bit-precision engine*, which scans data elements of evicted cache lines, identifies the largest data value across all data elements and updates the stored *maximum value* entry in the data transposition unit.

**$\mu$ Program Select Unit.** *Proteus*’s  *$\mu$ Program select unit* (③ in Fig. 4) aims to identify appropriate bit-precision for a PUD operation based on its input data. The  *$\mu$ Program select unit* consists of a (i) *bit-precision calculator unit*, which evaluates the target bit-precision based on the input operands of the target PUD operation and their associated maximum values, and (ii) buffer space to store the selected  $\mu$ Program.

### 4.2. Execution Flow

*Proteus* works in five main steps. In the first step (④ in Fig. 4), the programmer/compiler utilizes specialized instructions (i.e., *bbop* instructions) to (i) register to the *object tracker* the address, size, and initial bit-precision of memory objects of input, output, and temporary operands of a PUD operation; and (ii) execute PUD operations over previously-registered mem-

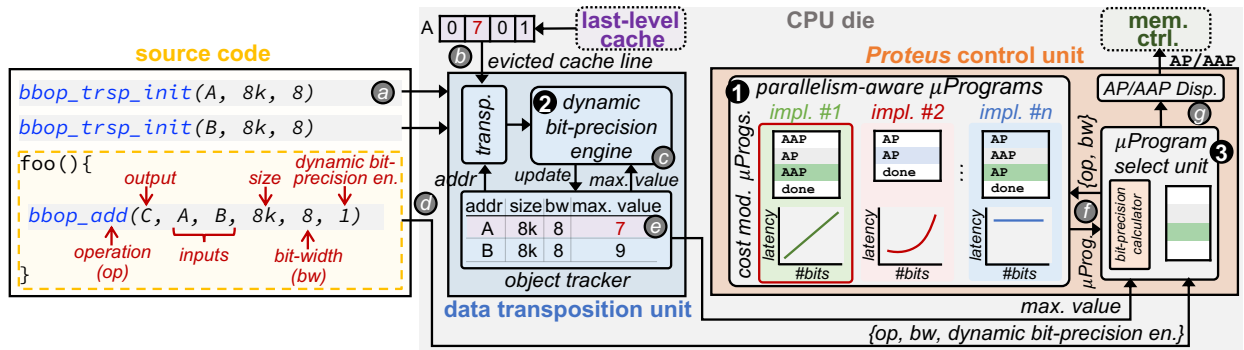


Figure 4: Overview of the Proteus framework.

ory objects. When issuing a *bbop* instruction, the programmer/compiler indicates whether or not dynamic bit-precision is enabled or disabled. When dynamic bit-precision is disabled, *Proteus*'s *dynamic bit-precision engine* is turned off, and the  $\mu$ Program *select unit* utilizes the user-provided bit-precision for upcoming PUD operations. In the second step, if the *dynamic bit-precision engine* is enabled, it intercepts evicted cache lines belonging to previously registered memory objects (b) and identifies the largest value stored in the cache line. If the identified value is *larger than* the current maximum stored in the *object tracker*, the *dynamic bit-precision engine* updates the *object tracker* with the up-to-date value (c). This process repeats for all cache lines of the registered memory objects. As in SIMDRAM [142], our system employs lazy allocation and data coherence for PUD memory objects is maintained via cache line flushing (using the *clflush* instruction [180]).<sup>3</sup> Thus, all memory objects initially reside within the CPU caches, and prior to PUD execution, all cache lines belonging to a PUD operation will be evicted to DRAM, which allows *Proteus*'s *dynamic bit-precision engine* to access *all* data elements of a PUD operation prior to computation.<sup>4</sup> In the third step, the host CPU dispatches *bbop* instructions (d) to *Proteus*'s control unit, alongside the maximum values of each input operand (e). In the fourth step, *Proteus*'s control unit receives the *bbop* instruction (from the CPU) and the maximum values (from the *dynamic bit-precision engine*), which are used as input to the  $\mu$ Program *select unit*. Based on such information, the *bit-precision calculator unit* computes the target bit-precision and probes the *parallelism-aware  $\mu$ Program library* (f), which returns the best-performing  $\mu$ Program and data format representation for the target operation and target bit-precision. In the fifth step, the  $\mu$ Program *select unit* dispatches the sequence of AAPs/APs in the selected  $\mu$ Program (g), finally realizing the target PUD operation. When the host CPU reads back PUD memory objects (not shown in the figure), *Proteus* (i) performs the necessary data format conversions either from the reduced bit-precision to the user's specified bit-precision or from RBR

to 2's complement (thus maintaining system compatibility), and (ii) prepares the *dynamic bit-precision engine* for future accesses by resetting the current maximum data value stored in the *object tracker*.

## 5. Proteus Implementation

In this section, we describe the implementation details of *Proteus*'s main components. We first describe *Proteus*'s underlying subarray organization (Section 5.1). Then, we discuss the design of *Proteus*'s (i) *parallelism-aware  $\mu$ Program library* (Section 5.2), (ii) *dynamic bit-precision engine* (Section 5.3), and (iii)  $\mu$ Program *select unit* (Section 5.4).

### 5.1. Subarray Organization

**Performing Logic Primitives with Ambit.** *Proteus* reuses the subarray organization of Ambit [101] and SIMDRAM [142] to enable logic primitive execution with only minimal subarray modifications. DRAM rows are divided into three groups: (i) the Data group (D-group), containing regular rows that store program data; (ii) the Control group (C-group), containing two rows pre-initialized with all-0 and all-1 values, use to control in-DRAM computation; and (iii) the Bitwise group (B-group), containing six rows (called *compute rows*) to perform bitwise operations. The B-group rows are all connected to a special row decoder that can simultaneously activate three rows when performing an AP and two when performing an AAP (1 in Fig. 5).

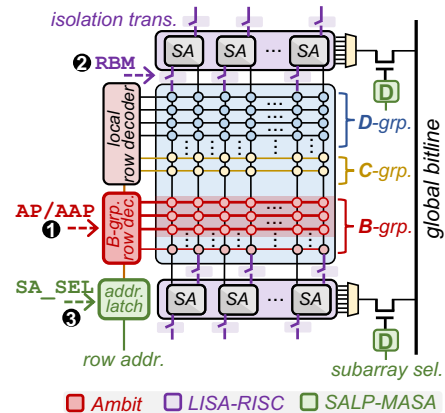


Figure 5: Subarray organization.

<sup>3</sup>The *clflush* instruction evicts the cache line containing the target memory address from *all* levels of the cache hierarchy [180]. Thus, even in case of non-inclusive caches, the target cache line will be flushed to DRAM.

<sup>4</sup>Loosely-coupled real-world PNM architectures [15, 19, 181] employ a similar execution model, where *all* input data needs to be copied and transposed to the PNM cores *prior* to PNM execution.

**Inter-Subarray Data Copy with LISA.** *Proteus* leverages LISA-RISC [152], which dynamically connects adjacent subarrays using isolation transistors, to propagate intermediate data across subarrays. LISA-RISC works in four steps: (i) activate the source row in the source subarray (latency:  $t_{RAS}$ ); (ii) use the LISA *row buffer movement* (RBM, ② in Fig. 5) command to turn on isolation transistors, which copies data from the source subarray’s local row buffer (LRB) to the destination subarray’s LRB (latency:  $t_{RBM}$ , 5 ns [152]); (iii) activate the destination row, to save the contents of the destination LRB into the row (latency:  $t_{RAS}$ ); and (iv) precharge the bank (latency:  $t_{RP}$ ). Due to DRAM’s open bitline architecture [150, 151], each LRB stores half of the row, so we must perform steps (ii)–(iv) twice to copy both halves of the row, resulting in a total latency of  $3t_{RAS} + 2t_{RP} + 2t_{RBM}$ .

**Enabling Subarray-Level Parallelism with SALP.** To enable the concurrent execution of data-independent steps in a  $\mu$ Program, *Proteus* leverages subarray-level parallelism (SALP) [182]. SALP-MASA (*multitude of activated subarrays*) allows multiple subarrays in a bank to be activated concurrently by (i) pushing the global row-address latch to individual subarrays, (ii) adding a designated-bit latch (D in Fig. 5) to each subarray to ensure that only a single subarray’s row buffer is connected to the global bitline, and (iii) routing a new global wire (called *subarray select*), controlled by a new DRAM command (SA\_SEL, ③ in Fig. 5), allowing the memory controller to set/clear each designated-bit latch.

## 5.2. Parallelism-Aware $\mu$ Program Library

**5.2.1. One-Bit Per-Subarray (OBPS) Data Mapping.** To reduce the latency of PUD operations (§3), *Proteus* employs a specialized data mapping called *one-bit per-subarray* (OBPS). Bit-serial PUD architectures can employ three data mappings, as Fig. 6 illustrates: all-bits in one-subarray (ABOS), all-bits per-subarray (APBS), and OBPS. Assume an example DRAM bank with four subarrays. (1) The ABOS maps all data to a single subarray, limiting data parallelism to the number of columns simultaneously computed by a single PUD primitive (e.g., 65,536 input operands per cycle). (2) The APBS stores multiple sets of operands across multiple subarrays, allowing PUD primitives to execute concurrently in each subarray (e.g.,  $4 \times 65,536$  input operands per cycle). (3) OBPS, distributes each bit of an operand to a different subarray, providing a new opportunity to extract the equivalent of instruction-level parallelism across independent PUD primitives within a single set of operands. For example, in an addition operation, any PUD primitive that does *not* need carry information can execute across all operand bits *simultaneously*. In OBPS, the parallelism the PUD substrate can leverage is a multiple of the number of DRAM subarrays used for computation divided by the target bit-precision, e.g.,  $\frac{4 \text{ subarrays}}{2 \text{ bits}} \times 65,536$  input operands per subarray.<sup>5</sup> Even though the parallelism available when employing OBPS data mapping is lower than the paral-

<sup>5</sup> If the number of subarrays is lower than the target bit-precision, OBPS evenly distributes the bits of input operands across the available subarrays.

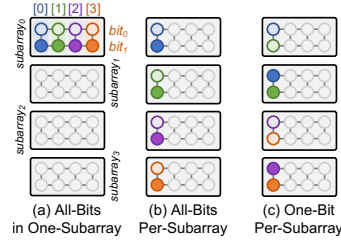


**Figure 6: Three data mappings for bit-serial computing.**

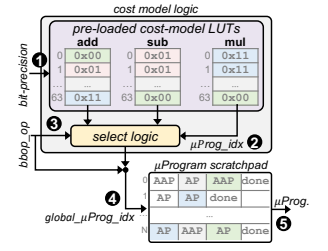


**Figure 7: *Proteus*'s cost model logic.**

lism available when only employing APBS, the OBPS data mapping allows *Proteus* to parallelize independent instructions in a  $\mu$ Program, which can lead to latency reduction.

**5.2.2.  $\mu$ Program Library Implementation.** *Proteus* leverages the subarray organization illustrated in Fig. 5 and our OBPS data mapping to implement parallelism-aware  $\mu$ Programs for key arithmetic operations. We implement three classes of algorithms for arithmetic PUD computations: *bit-serial*, *bit-parallel*, and *RBR-based algorithms*. In *Proteus*, each  $\mu$ Program implementation (i) has an associated *global\_muProgram\_idx*, and (ii) is stored in a reserved memory space in DRAM (i.e., *muProgram memory*).

**Bit-Serial Algorithms.** We optimize  $\mu$ Programs for bit-serial arithmetic operations (i.e., addition, subtraction, division, and multiplication) by concurrently executing independent AAPs/APs across different DRAM subarrays. Fig. 3b illustrates such a process for addition (the process is analogous for other arithmetic operations). *Proteus* implements a ripple-carry adder using majority gates in two main steps. First, *Proteus* utilizes SALP-MASA to concurrently execute the appropriate row copies and majority operations across  $N$  different subarrays. Second, *Proteus* utilizes LISA-RISC to pipeline the carry propagation process from *subarray<sub>i</sub>* (e.g.,  $C_{out}^0$ ) to *subarray<sub>i+1</sub>* (e.g.,  $C_{in}^1$ ). This process repeats for all  $N$  bits in the input operand. *Proteus* reduces the latency of executing bit-serial addition from  $8N + 1$  AAP/AP cycles to  $2N + 7$  AAP/AP cycles +  $2(N - 1)$  RBM cycles.<sup>6</sup>

**Bit-Parallel Algorithms.** We implement bit-parallel variants of our  $\mu$ Programs that leverage *carry-lookahead logic* to decouple the calculation of the carry bits and arithmetic logic (e.g., addition). Carry-lookahead logic can identify if any arithmetic on a bit will *generate* a carry (e.g., both operands bits are ‘1’ for an addition), or if it will *propagate* the carry value (e.g., only one operand bit for an addition is a ‘1’). For  $n$ -bit operands, this reduces time complexity compared to ripple-carry logic from  $\mathcal{O}(n)$  to  $\mathcal{O}(\log n)$ . We implement several carry-lookahead algorithms in *Proteus*, including the carry-select [183], Kogge–Stone [184], Ladner–Fischer [185], and Brent–Kung [186] adders, as building blocks to implement subtraction, multiplication, and division. Fig. 8a shows an example *Proteus* implementation of a Kogge–Stone adder.

<sup>6</sup>To compute the number of AAP/AP and RBM cycles in a  $\mu$ Program, we implemented each  $\mu$ Program’s algorithm using our in-house cycle-/data-accurate simulator (see §6). We verified the correctness of a  $\mu$ Program by testing it against several randomly generated data set combinations.

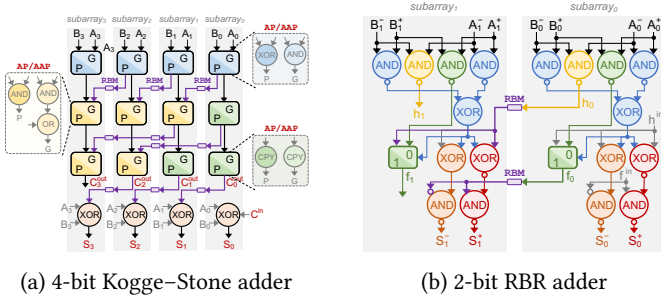


Figure 8: *Proteus*'s implementation of different adders. Bits  $A_i$  and  $B_i$  are stored vertically in the same DRAM bitline.

In the first step, *Proteus* performs several inter-subarray data copies (using LISA-RISC) to copy the *generate* and *propagate* bits from  $subarray_i$  to  $subarray_{i+1}$ . In the second step, *Proteus* performs a series of Boolean operations (using AAPs/APs) to compute the next generate and propagate bits in parallel (using SALP-MASA) across *all* DRAM subarrays. These two steps repeat for  $\log(n)$  iterations, where  $n$  is the number of bits in the input operands. Compared to SIMDRAM, *Proteus* reduces the latency of executing bit-serial addition from  $8N + 1$  AAP/AP cycles to  $(3\log_2 N + 13)$  AAP/AP cycles +  $(2N + 4)$  RBM cycles. Even though the bit-parallel algorithms have a lower time complexity than the bit-serial algorithms, the latter can require more inter-subarray copies.

**RBR-Based Algorithms.** Fig. 8b illustrates *Proteus*'s implementation of a two-bit RBR-based adder [187]. In this adder, the intermediate output  $h_i$  is a function of digit  $i$ . The output  $f_i$  is a function of digit  $i$  and  $h_{i-1}$ . The sum of digit  $i$  is a function of digit  $i$ ,  $h_{i-1}$ , and  $f_{i-1}$ . *Proteus* uses RBM commands to copy the intermediate digits  $h_i$  and  $f_i$  from  $subarray_i$  to  $subarray_{i+1}$ . *Proteus* performs RBR-based addition with a fixed latency of 34 AAPs/APs cycles and 8 RBM cycles. *Proteus* leverages the RBR-based adder to perform other operations in RBR format, such as subtraction and multiplication.

**5.2.3. Cost Model Logic Implementation.** Fig. 7 depicts the hardware design of the *cost model logic*. The *cost model logic* has two main components: (i) one LUT per PUD operation, and (ii) select logic. Each LUT row represents a different bit-precision, and stores the index of the best-performing  $\mu$ Program in the library for that operation/precision. A LUT contains 64 eight-bit rows (i.e., supporting up to 64-bit computation, and indexing up to 64 different  $\mu$ Program implementations per PUD operation). The *cost model logic* works in four main CPU cycles (taking into account in our evaluation). It receives as input the *bit-precision* (6 bits) and the *bbop\_op* opcode (4 bits) of the target PUD operation. In the first cycle, the *bit-precision* indexes all the LUTs in parallel (1 in Fig. 7), selecting the best-performing  $\mu$ Program\_idx for the given bit-precision for all implemented PUD operations (2). The *cost model logic* can quickly query the LUTs since they consist of a few (i.e., 16) small (i.e., 64 B in size) SRAM arrays indexed in parallel. In the second cycle, based on the 4-bit *bbop\_op* opcode, the selector logic selects the appropriate  $\mu$ Program\_idx (3). In the third cycle, the  $\mu$ Program\_idx is concatenated with the

*bbop\_op* opcode to form the *global\_μProgram\_idx* (4). In the fourth cycle, the *global\_μProgram\_idx* indexes and fetches the best-performing  $\mu$ Program from the *μProgram scratchpad* (5). If the target  $\mu$ Program is not loaded in the *μProgram scratchpad*, the *cost model logic* fetches it from the *μProgram memory* (not shown). We estimate, using CACTI [188], that the access latency and energy per access of the 64 B SRAM array (used in our *cost model logic*) is of 0.07 ns (i.e., less than 1 CPU cycle) and 0.000 04 nJ.

**5.2.4. Pareto Analysis.** To populate the cost-model LUTs with the best-performing  $\mu$ Program implementation for a given PUD operation, we conduct a performance and energy Pareto analyses. We model each  $\mu$ Program using an analytical cost model that takes as input the target bit-precision, the number of elements used during computation, and the number of DRAM subarrays available. The analytical cost model outputs the throughput (in GOPs/s) and energy efficiency (in throughput/Watt) for each  $\mu$ Program in the *parallelism-aware μProgram library*. We highlight our analyses for two main operations (i.e., addition and multiplication) since they represent linearly and quadratically scaling PUD operations, respectively. The analyses for subtraction and division follow similar observations. In our analyses, we evaluate a SIMDRAM-like PUD architecture using the three data mapping schemes described in Fig. 6. We assume a DRAM bank with 64 DRAM subarrays capable of in-DRAM computing and a subarray with 65,536 columns. We vary the number of input elements as multiples of the number of DRAM columns per subarray (from 1 DRAM subarray with 64 K input elements to 64 DRAM subarrays with 4 M input elements) to obtain the steady-state for our measurements.

**Linearly Scaling PUD Operations.** Fig. 9 shows the throughput (top) and energy efficiency (bottom) of six  $\mu$ Program implementations for a linearly scaling PUD operation (i.e., addition). We make two observations. First, regarding throughput, we observe that the best-performing adder implementation varies depending on the target bit-precision and number of input elements. For small bit-precision and small input size (i.e., bit-precision smaller than 8, and less than 256 K input elements), the bit-serial RCA using the OBPS data mapping provides  $2.7\times$  ( $1.4\times$ ) the throughput of ABOS (APBS) addition implementation. For large bit-precision and small input size (i.e., bit-precision larger than 8, and less than 256 K input elements), the RBR adder using the OBPS data mapping provides  $7.7\times$  ( $3.9\times$ ) the throughput of ABOS (APBS) addition implementation. For large-enough input sizes (i.e., larger than 4 M input elements), employing the APBS data mapping leads to the highest throughput, independent of the target bit-precision. This is because when more DRAM subarrays are involved in the execution of the target PUD operation, the inter-subarray data transfers dominate overall execution time in the OBPS implementations. Second, regarding energy efficiency, the bit-serial implementation of the RCA provides the best throughput per Watt for ABOS, APBS, and OBPS, independent of the target bit-precision and input size. This is because (i) the number of AAPs/APs performed to execute the

RCA is the same *independent* of the data mapping, and (ii) the energy the bit-parallel algorithms consume is dominated by inter-subarray operations.

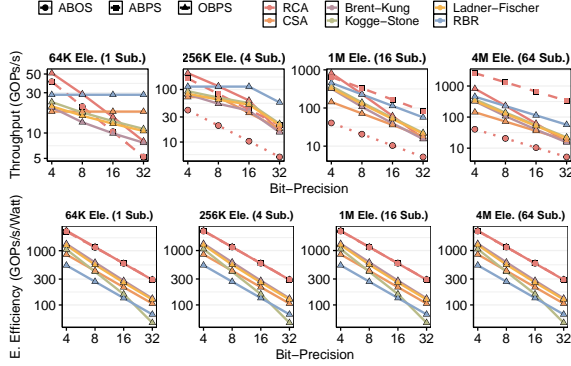


**Figure 9: Pareto analysis for throughput (top) and energy efficiency (bottom) for PUD addition operations. Dotted lines represent the ABOS; dashed lines represent the APBS; straight lines represent the OBPS data mapping.**

**Quadratically Scaling PUD Operations.** Fig. 10 shows the throughput (top) and energy efficiency (bottom) of six  $\mu$ Program implementations for a quadratically scaling PUD operation (i.e., multiplication). For this analysis, we implement multiplication using two multiplication methods (i.e., the standard grade-school multiplication and the divide-and-conquer Karatsuba [189] multiplication) using three different methods for addition (i.e., bit-serial RCA, bit-parallel Ladner-Fischer [185], and the RBR adder in Fig. 8b). We make two observations from the figure. First, regarding throughput, similar to the linearly scaling Pareto analysis, we observe that the best-performing multiplier implementation varies depending on the target bit-precision and number of input elements. For small bit-precision and small input size (i.e., bit-precision smaller than 8, and less than 64 K input elements), ABOS’s implementation of the standard bit-serial multiplication provides the highest throughput. For medium bit-precision and small input size (i.e., bit-precision from 8 to 16 and less than 64 K input elements), OBPS’s implementation of the standard bit-parallel multiplication provides the highest throughput, i.e.,  $1.5\times$  ( $1.5\times$ ) the throughput of ABOS (APBS) multiplication implementation. For high bit-precision and small-to-medium input size (i.e., bit-precision larger than 32 and less than 256 K input elements), OBPS’s implementation of the RBR multiplication provides the highest throughput, i.e.,  $4\times$  ( $2\times$ ) the throughput of ABOS (APBS) multiplication implementation. Similar to the addition case, for large-enough input sizes (i.e., larger than 1 M input elements), employing the APBS data mapping leads to the highest throughput, independent of the target bit-precision. Second, regarding energy efficiency, the standard bit-serial multiplication implementation provides the best throughput per Watt for ABOS, APBS, and OBPS, independent of the target bit-precision and input size.

**5.2.5. Non-Arithmetic PUD Operations..** We also equip *Proteus’s* *parallelism-aware*  $\mu$ Program library with SIMDRAM’s implementations of non-arithmetic PUD operations, including

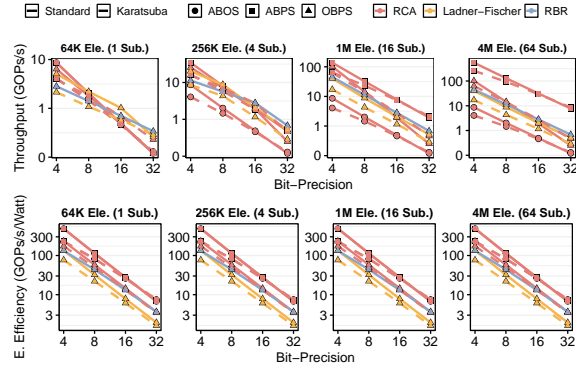


**Figure 10: Pareto analysis for throughput (top) and energy efficiency (bottom) for multiplication. Dashed lines represent the standard multiplication method; straight lines represent the Karatsuba [189] multiplication method.**

(i)  $N$ -bit logic operations (i.e., AND/OR/XOR of more than two input bits), (ii) relational operations (i.e., equality/inequality check, greater than, maximum, minimum), (iii) predication, and (iv) bitcount and ReLU [190].

### 5.3. Dynamic Bit-Precision Engine

The *dynamic bit-precision engine* comprises a simple reconfigurable  $n$ -bit comparator and a finite state machine (FSM). For each evicted cache line, the FSM probes the *object tracker* and identifies if the upcoming cache line belongs to a PUD’s memory object. If it does, the FSM executes four operations. First, it reads the bit-precision value (specified by the `bbop_trsp_init` instruction) and the current maximum value stored in the *object tracker* for the given memory object. Second, it uses the bit-precision value to configure the  $n$ -bit comparator. Third, it inputs to the  $n$ -bit comparator all  $n$ -bit values in the upcoming cache line (one per time) and the current maximum value. Fourth, after all the  $n$ -bit values are processed, if any value in the upcoming cache line is larger than the current maximum value, the FSM sends an update signal to the *object tracker* alongside the new maximum value. The energy cost of identifying the largest element in a 64 B cache line is 0.0016 nJ [191]. That represents an increase in 0.084% in the energy of an LLC eviction [81, 192, 193], which *needs* to happen prior to PUD execution regardless.

### 5.4. $\mu$ Program Select Unit

**Calculating Bit-Precision.** The  *$\mu$ Program select unit* needs to address two scenarios when calculating the bit-precision for PUD operations: *vector-to-vector* PUD operations, and *vector-to-scalar* reduction PUD operations. In the first scenario, the target PUD operation implements a parallel *map* operation, in which inputs and outputs are data vectors. For such operations, the bit-precision can be computed *a priori*, using the maximum values the *dynamic bit-precision engine* provides, *even* in the presence of chains of PUD operations. In such a case, the *bit-precision calculator* engine updates the *object tracker* with the maximum possible output value for *each* PUD in the chain. For example, assume a kernel that executes  $D[i]=(A[i]+B[i])\times C[i]$  as follows:



```

bbop_add(tmp, A, B, 8k, 8, 1); // tmp ← A + B
bbop_mul(D, tmp, C, 8k, 8, 1); // D ← tmp × C

```

Assume that the maximum value of A, B, and C are 3, 6, and 2, respectively. In this case, the  $\mu$ Program select unit (i) computes the bit-precision for the addition operation as  $\lceil \log_2(3 + 6) \rceil = 4$  bits; (ii) updates the *object tracker* entry of tmp with the maximum value of the addition operation (i.e., 9); (iii) computes the bit-precision for the multiplication operation as  $\lceil \log_2(9 \times 2) \rceil = 5$  bits using a reconfigurable  $n$ -bit scalar ALU; (iv) updates the *object tracker* entry of D with the maximum value of the multiplication (i.e., 18).

In the second scenario (*vector-to-scalar* reduction), the PUD operation implements a parallel *reduction* operation, where the inputs are vectors and the output is a scalar value. In this case, the bit-precision *cannot* be computed with *only* the maximum input operands without causing *overprovision*, since in a reduction, each element contributes to the bit-precision of the scalar output. Therefore, for *vector-to-scalar* reduction PUD operations, the  $\mu$ Program select unit needs to (i) fetch from DRAM the row containing the carry-out bits produced during partial steps<sup>7</sup> of the PUD reduction; (ii) evaluate if a partial step generated an overflow (i.e., check if any carry-out bit is ‘1’); and (iii) increment the bit-precision for the next partial step in the case of an overflow. We design the  $\mu$ Program select unit to fully overlap the latency of bit-precision computation with  $\mu$ Program execution.

**Hardware Design.** The  $\mu$ Program select unit comprises of simple hardware units: (i) a reconfigurable  $n$ -bit ALU to compute the target bit-precision, (ii) a *fetch unit* to generate load instructions for carry re-evaluation, and (iii) a  $\mu$ Program buffer to store the currently running  $\mu$ Program.

## 5.5. Putting It All Together

**Data Format Conversion.** To distribute the bits of input operands to different DRAM subarrays, *Proteus* issues RBM commands from the DRAM row storing bit  $i$  in the source DRAM subarray to the target DRAM row in the destination DRAM subarray  $i$ , i.e.,  $row[dst]_{subarray_i} \leftarrow RBM(row[src]_i); i \in [1, bits]$ . To convert the data stored in 2’s complement to its equivalent RBR (see §3), *Proteus* performs in-DRAM bitwise operations, as Table 1 describes.

**Table 1: Data conversion from 2’s complement to RBR.**

| Input X →<br>2’s complement →           | 2        | -1      | -7      |
|---|----------|---------|---------|
|   | 0 0 1 0  | 1 1 1 1 | 1 0 0 1 |
| Steps to convert 2’s to RBR ↓           | Output ↓ |         |         |
| Extract most-significant bit (MSB)      | 0        | 1       | 1       |
| -buffer: broadcast MSB to all subarrays | 0 0 0 0  | 1 1 1 1 | 1 1 1 1 |
| +buffer: NOT(-buffer)                   | 1 1 1 1  | 0 0 0 0 | 0 0 0 0 |
| X + 1                                   | 1 1 1 0  | 0 0 0 1 | 0 1 1 1 |
| X - = -buffer & (X + 1)                 | 0 0 0 0  | 0 0 0 1 | 0 1 1 1 |
| X + = +buffer & (X)                     | 0 0 1 0  | 0 0 0 0 | 0 0 0 0 |

<sup>7</sup>*Proteus* implements PUD reduction operations using *reduction trees* [141]. Thus, a partial step refers to a level of the reduction tree.

**System Integration.** *Proteus* leverages the *same* system integration solutions as in prior PUD systems [141, 142], including: (i) ISA extensions included to the host CPU ISA that the programmer utilizes to launch *bbop* instructions; (ii) a hardware control unit, alongside the memory controller, to control the execution of  $\mu$ Programs; and (iii) a hardware transposition unit, placed between the LLC and the memory controller, to transpose data from the native horizontal data layout to the PUD-friendly vertical data layout. As in [141, 142], we assume that the operating system (OS) can provide support for data allocation and data mapping of operands in the DRAM bank dedicated for PUD computing and the PUD substrate operates directly on physical addresses.

**Limitation of SALP.** SALP is limited by the  $t_{FAW}$  DRAM timing constant [194–196], which corresponds to the time window during which at most four ACT commands can be issued per DRAM rank. This constraint protects against the deterioration of the DRAM reference voltage. DRAM manufacturers have been able to relax  $t_{FAW}$  substantially in commodity DRAM chips [197], as well as to perform a targeted reduction of this parameter specifically for PIM architectures where it becomes a performance bottleneck [70, 198]. These advances suggest that this parameter may *not* limit *Proteus*’s scalability severely in commodity DRAM chips.

## 5.6. Proteus for Floating-Point Operations

Prior PUM works [113, 121, 199] have demonstrated how IEEE 754 floating-point operations can be realized in bit-serial in-memory computing engines. Since narrow values are also present in floating-point data [153, 171, 200], such works could benefit from the dynamic bit-precision ideas we introduce in *Proteus*. Concretely, *Proteus*’s dynamic bit-precision computation can be employed in two different steps of floating-point arithmetic: during exponent and mantissa computation.<sup>8</sup> In either case, the first step is to enable the programmer/compiler to communicate to *Proteus* control unit that the target PUD instruction uses floating-point data. To do so, we need to extend the PUD ISA (i.e., the *bbop\_op* instructions in Fig. 4; left) to identify if the inputs of the target PUD operation are stored in integer, single-precision (floating-point), or double-precision (double) format. *Proteus* then exploits narrow values in floating-point PUD operations in three main steps.

First, the *dynamic bit-precision engine* identifies the sign, exponent, and mantissa bits in floating-point numbers stored in the evicted cache lines of PUD memory objects. Second, the *dynamic bit-precision engine* updates the *object tracker* with the maximum exponent and the mantissa values for the PUD memory object, in case the current stored maximum values are smaller than the values stored in the current evicted cache line. This process is analogous to the execution flow described in §4.2 for integer operands, with the addition of the fields for

<sup>8</sup>The IEEE 754 single-precision floating-point format [201] is a 32-bit binary representation that encodes a floating-point number in three distinct parts: (i) sign bit (1 bit), (ii) exponent (8 bits), and (iii) mantissa (23 bits). The structure of a single-precision floating-point number can be written as:  $(-1)^{sign} \times 1.mantissa \times 2^{exponent-127}$ .

the maximum exponent and maximum mantissa values in the *object tracker*. Third, *Proteus* performs the target in-memory floating-point computation by issuing [113] (i) bit-serial subtraction (addition) PUD operations to calculate the resulting exponents, followed by (ii) bit-serial addition (multiplication) PUD operations to calculate the resulting mantissas for a vector addition (multiplication) instruction [113]. Note that the bit-serial PUD operations involved in (i)–(ii) are vector-to-vector PUD operations. As such, *Proteus* can leverage the maximum exponent and mantissa values stored in the *object tracker* to set the required bit-precision for such bit-serial operations, following the same approach described in §5.4.

We identify another opportunity to exploit narrow values during mantissa computation by identifying *repeating patterns* in the mantissa to configure the bit-precision for the target operation. For example, when representing +1.3 in floating-point (sign = ‘0’, exponent = ‘01111111’, mantissa = ‘01001100110011001100110’), the mantissa bits ‘0011’ repeats five times. Based on that, we can perform the bit-serial mantissa computation by (i) issuing PUD operations (e.g., adding or multiplying the mantissa) for the first iteration of the repeating pattern ‘0011’ and (ii) copying (using RowClone [104]) the remaining bits of the output mantissa depending on the identified repeating pattern (i.e., four times in our example). However, to implement such a scheme, *Proteus* would need to identify variable-length patterns across the mantissa bits for all data elements involved in the computation, which would incur non-trivial hardware complexity. Thus, we leave the realization of this optimization approach as future work.

## 6. Methodology

We implement *Proteus* using an in-house cycle-level simulator and compare it to a real multicore CPU (Intel Comet Lake [202]), a real high-end GPU (NVIDIA A100 using CUDA and tensor cores [203]), and a simulated state-of-the-art PUD framework (SIMDRAM [142]). In all our evaluations, the CPU code uses AVX-512 instructions [204]. Our in-house simulator was rigorously validated against SIMDRAM [142] and MIMDRAM [141]’s gem5 [205] implementation [206]. The simulator (i) is cycle-level accurate with regard to DRAM commands (i.e., ACT/RD/PRE DRAM commands) and (ii) follows the gem5 cache model, i.e., it accounts for the data movement cost of cache line eviction on a per-cycle basis. Our simulation accounts for the additional latency imposed by SALP [182] on ACT commands, i.e., the extra circuitry required to support SALP incurs an extra latency of 0.028 ns to an ACT [207], which is less than 0.11% extra latency for an AAP. To verify the functional correctness of our applications, our simulation infrastructure perform functional verification over application’s data when performing PUD operations. We did *not* observe any difference from the golden outputs.

Table 2 shows the system parameters we use in our evaluations. To measure CPU energy consumption, we use Intel RAPL [208]. We capture GPU kernel execution time that excludes data initialization/transfer time. We use the

Table 2: Evaluated system configurations.

|                               |  |
|-------------------------------|--|
| Intel<br>Comet Lake CPU [210] | x86 [180], 16 cores, 8-wide, out-of-order, 3.8 GHz;<br>L1 Data + Inst. Private Cache: 256 kB, 8-way, 64 B line;<br>L2 Private Cache: 2 MB, 4-way, 64 B line;<br>L3 Shared Cache: 16 MB, 16-way, 64 B line;<br>Main Memory: 64 GB DDR4-2133, 4 channels, 4 ranks  |
| NVIDIA<br>A100 GPU [203]      | 7 nm technology node; 826 mm <sup>2</sup> die area [203]; 6912 CUDA cores;<br>432 tensor cores, 108 streaming multiprocessors, 1.4 GHz base clock;<br>L2 Cache: 40 MB L2 Cache; Main Memory: 40 GB HBM2 [211, 212]   |
| SIMDRAM [142]<br>& Proteus    | gem5-based in-house simulator; x86 [180];<br>1 out-of-order core @ 4 GHz (only for instruction offloading);<br>L1 Data + Inst. Cache: 32 kB, 8-way, 64 B line;<br>L2 Cache: 256 kB, 4-way, 64 B line;<br>Memory Controller: 8 kB row size, FR-FCFS [213, 214]<br>Main Memory: DDR5-5200, 1 channel, 1 rank, 16 banks |

nvml API [209] to measure GPU energy consumption. We use CACTI [188] to evaluate *Proteus* and SIMDRAM energy consumption, where we take into account that each additional simultaneous row activation increases energy consumption by 22% [101, 142]. We evaluate two SIMDRAM configurations: (i) SIMDRAM with SALP and static bit-precision (*SIMDRAM-SP*), and (ii) SIMDRAM with SALP and *Proteus*’s dynamic bit-precision engine (*SIMDRAM-DP*). In both configurations, the system implements only the 16  $\mu$ Programs proposed in SIMDRAM (i.e., there is *no parallelism-aware  $\mu$ Program library* enabled). We evaluate four *Proteus* configurations: (i) *Proteus LT-SP* and (ii) *Proteus EN-SP*, where *Proteus* selects the *lowest latency* and *lowest energy* consuming  $\mu$ Program, respectively, using the statically profiled bit-precision from Fig. 2; (iii) *Proteus LT-DP* and (iv) *Proteus EN-DP*, where *Proteus* executes the *lowest latency* and *lowest energy* consuming  $\mu$ Program with dynamically chosen bit-precision. We use 64 subarrays in one DRAM bank for PUD.<sup>9</sup>

**Real-World Applications.** We select twelve workloads from four popular benchmark suites in our real-workload analysis (as Table 3 describes). We manually modified each workload to (i) identify loops that can benefit from PUD computation, i.e., loops that are memory-bound and that can leverage single-instruction multiple-data (SIMD) parallelism and (ii) use the appropriate *bbop* instructions. To identify loops that can leverage SIMD parallelism, we follow the compilation steps the authors of [141] propose, which uses LLVM’s loop auto-vectorization engine [167–170] as a profiling tool that outputs SIMD-safe loops in an application. We use the clang compiler [167] to compile each application while enabling the loop auto-vectorization engine and its loop vectorization report (i.e., -O3 -Rpass-analysis=loop-vectorize -Rpass=loop-vectorize). We observe that applications with regular and wide data parallelism (e.g., applications operating over large dense vectors) are better suited for SIMD-based PUD systems. Based on that, we select applications from various domains, including linear algebra and stencil computing (i.e., 2mm, 3mm, doitgen, fdtd-apml, gemm, gramschmidt from Polybench [215]), machine learning (i.e., pca from Phoenix [216], covariance from Polybench [215], kmeans and backprop from Rodinia [217]), and image/video processing (i.e., heartwall from

<sup>9</sup>The column/address (C/A) bus allows the simultaneous activation of up to 84 DRAM subarrays ( $\frac{t_{RAS}}{t_{CK}} = \frac{32 \text{ ns}}{0.38 \text{ ns}} = 84$ ).

Rodinia [217] and 525.x264\_r from SPEC 2017 [218]).<sup>10</sup> Since our base PUD substrate (SIMDRAM) does *not* support floating-point, we manually modify the selected floating-point-heavy PUD-friendly loops to operate on fixed-point data arrays.<sup>11</sup> We do *not* observe an output quality degradation when employing fixed-point for the selected loops. We use the largest input dataset available.

**Table 3: Evaluated applications and their characteristics.**

| Benchmark Suite | Application (Short Name) | Peak GPU Util. (%) | Total Mem. Footprint (GB) | Bit-Precision (min, max) | PUD Instrs. <sup>†</sup> |
|-----------------|--------------------------|--------------------|---------------------------|--------------------------|--------------------------|
| Phoenix [216]   | pca (pca)                | -                  | 1.91                      | {8, 8}                   | D, S, M, R               |
|                 | 2mm (2mm)                | 98                 | 4.77                      | {13, 25}                 | M, R                     |
|                 | 3mm (3mm)                | 100                | 26.7                      | {12, 12}                 | M, R                     |
| Polybench [215] | covariance (cov)         | 100                | 7.63                      | {23, 23}                 | D, S, R                  |
|                 | doitgen (dg)             | 92                 | 33.08                     | {10, 11}                 | M, C, R                  |
|                 | fdtd-apml (fdtd)         | -                  | 36.01                     | {11, 13}                 | D, M, S, A               |
|                 | gemm (gmm)               | 98                 | 22.89                     | {12, 24}                 | M, R                     |
|                 | gramschmidt (gs)         | 66                 | 22.89                     | {12, 13}                 | M, D, R                  |
| Rodinia [217]   | backprop (bp)            | -                  | 22.50                     | {13, 13}                 | M, R                     |
|                 | heartwall (hw)           | 48                 | 0.03                      | {17, 17}                 | M, R                     |
|                 | kmeans (km)              | 36                 | 1.23                      | {17, 17}                 | S, M, R                  |
| SPEC 2017 [218] | 525.x264_r (x264)        | -                  | 0.15                      | {1, 8}                   | A, R                     |

<sup>†</sup>: D = division, S = subtraction, M = multiplication, A = addition, R = add reduction, C = copy

## 7. Evaluation

### 7.1. Real-World Application Analysis

**Performance Analysis.** Fig. 11 shows the CPU, GPU, SIMDRAM, and *Proteus* performance for twelve real-world applications. As in prior works [103, 119, 120, 224, 225], we report area-normalized results (i.e., performance per  $\text{mm}^2$ ) for a fair comparison. We make four observations. First, *Proteus* significantly outperforms all three baseline systems. On average across all twelve applications, *Proteus LT-DP* (*Proteus EN-DP*) achieves  $17\times$  ( $11.2\times$ ),  $7.3\times$  ( $4.8\times$ ), and  $10.2\times$  ( $6.8\times$ ) the performance per  $\text{mm}^2$  of the CPU, GPU, and SIMDRAM, respectively. Second, we observe that equipping SIMDRAM with *Proteus*'s dynamic bit-precision engine to leverage narrow values for PUD execution significantly improves overall performance. On average, *SIMDRAM-DP* provides  $6.3\times$  the performance of *SIMDRAM-SP*. Third, *Proteus*'s ability to adapt the  $\mu$ Program depending on the target bit-precision further improves overall performance by  $1.6\times$  that of *SIMDRAM-DP*. Fourth, *Proteus*'s dynamic bit-precision engine further increases performance by  $46\%$ , compared to *Proteus* with static bit-precision. This happens because for statically profiled bit-precision, we *must* round the bit-precision up to the nearest power-of-two, since high-level programming language (e.g., C/C++) are *bounded* by  $2$ 's complement data representation formats.

**Energy Analysis.** Fig. 12 shows the GPU, SIMDRAM, and *Proteus* energy for twelve applications. Values are normalized to the CPU baseline. We make four observations. First,

<sup>10</sup>Note that PUD architectures are not yet general-purpose solutions that are (easily) well-suited for a very wide variety of workloads. The authors of [141] have conducted an extensive workload characterization analysis of 117 different applications from seven benchmark suites (SPEC 2017 [218], SPEC 2006 [219], Parboil [220], Phoenix [216], Polybench [215], Rodinia [217], and SPLASH-2 [221]) to identify kernels that are suited to PUD architectures, with results on the twelve same applications we utilize in our paper.

<sup>11</sup>We only modify the three applications from Rodinia to use fixed-point, as done by prior works [136, 222, 223]. Polybench can be configured to use integers; the PUD-friendly loops in x264 and pca use integers.

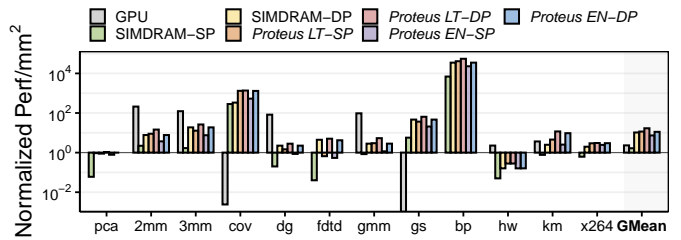


**Figure 11: CPU-normalized performance per  $\text{mm}^2$  for twelve real-world applications. Phoenix [216] and SPEC2017 [218] do not provide GPU implementations of pca and x264.**

*Proteus* significantly reduces energy consumption compared to all three baseline systems. On average across all twelve applications, *Proteus EN-DP* (*Proteus LT-DP*) reduces energy consumption by  $90.3\times$  ( $27\times$ ),  $21\times$  ( $6.3\times$ ), and  $8.1\times$  ( $2.5\times$ ) that of the CPU, GPU, and *SIMDRAM-SP*, respectively. Second, *Proteus*'s dynamic bit-precision engine and *parallelism-aware  $\mu$ Program library* enhance energy reduction by an average of  $8\times$  and  $1.02\times$  compared to *SIMDRAM-SP* and *SIMDRAM-DP*, respectively. Third, compared to *SIMDRAM-DP*, *Proteus LT-DP* increases energy consumption by  $3.3\times$ , on average. This is because the most performance-efficient implementation of a PUD operation often leads to an increase in the number of AAPs/APs required for PUD computing. In many cases, the energy associated with inter-subarray data copies (employed in RBR and bit-parallel algorithms) leads to an *increase* in energy consumption (§5.2.4). Even though the inter-subarray data copy latency can be hidden by leveraging *Proteus*'s OBPS data mapping, the extra power the DRAM subsystem requires to perform them impacts overall energy consumption. Fourth, the *dynamic bit-precision engine* further reduces *Proteus* energy consumption by  $58\%$ , compared to *Proteus* with static bit precision.

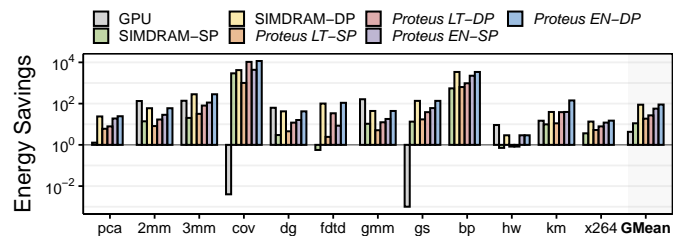


**Figure 12: Energy savings for twelve applications.**

### 7.2. Data Format Conversion Overhead

Fig. 13 shows the worst-case data format conversion latency for linearly- and quadratically-scaling  $\mu$ Programs. We make two observations. First, data format conversion can significantly impact linearly-scaling  $\mu$ Programs, leading to up to  $60\%$  and  $91\%$  overheads when converting from ABOS to OPBS and from ABOS to RBR, respectively. Second, in contrast, the impact of data format conversion in quadratically scaling  $\mu$ Programs is low (i.e., less than  $10\%$  latency overhead). This difference is because the number of in-DRAM operations required to perform data format conversion increases linearly with the bit-precision (§5.5). In most cases, the data format conversion is a one-time overhead that an application pays when execut-

ing a series of PUD operations. On average, across our 12 applications, data format conversion accounts for 7.2% of the total execution time.

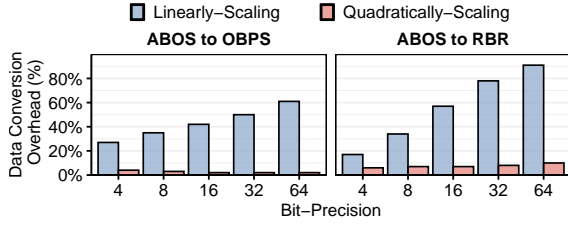


Figure 13: Data format conversion overhead.

### 7.3. Performance of Floating-Point Operations

We evaluate *Proteus*'s throughput for floating-point arithmetic operations. Since our underlying PUD architecture, i.e., SIMD-DRAM, does *not* natively support floating-point operations, we demonstrate how *Proteus* can be leveraged in a different PUD architecture that can be modified to support floating-point data formats, i.e., DRISA [103]. The main limitation of SIMD-DRAM when supporting floating-point computation is the lack of interconnects across DRAM columns, which is required for exponent normalization during floating-point addition. Since the DRISA architecture includes a shifting network within a DRAM subarray, it can perform the required exponent normalization.

We perform a synthetic throughput analysis of in-DRAM vector addition/subtraction and multiplication/division operations.<sup>12</sup> We use 64M-element input arrays, with randomly initialized single-precision floating-point data. We evaluate two system configurations: (i) DRISA 3T1C [103] architecture, which performs *in-situ* NOR computation; and (ii) DRISA 3T1C architecture coupled with *Proteus*. We make two observations. First, we observe that the DRISA 3T1C architecture coupled with *Proteus* achieves  $1.17\times/1.15\times$  and  $1.38\times/1.37\times$  the arithmetic throughput of the baseline DRISA 3T1C for floating-point addition/subtraction and multiplication/division operations, respectively. Second, *Proteus*'s throughput gains are more prominent for multiplication/division operations, since it can avoid costly in-memory multiplication/division operations during mantissa computation by leveraging narrow mantissa values. We conclude that *Proteus*'s key ideas apply to different underlying in-DRAM processing techniques and data formats.

### 7.4. Performance of *Proteus* vs. Tensor Cores in GPUs

Similar to *Proteus*, modern GPU architectures, such as our baseline NVIDIA A100 GPU, are also designed with narrow data precision in mind. In particular, the NVIDIA A100 GPU is equipped with *specialized* tensor core engines [203] designed *particularly* for high-throughput general matrix-matrix multiplication (GEMM) operations. To this end, in this section, we

<sup>12</sup>We evaluate synthetic workloads instead of our twelve real-world applications since there is *no* publicly available tool-chain to map real-world applications to the baseline DRISA [103] architecture. A similar approach is conducted in [142].

compare the performance and energy efficiency of a subset of our real-world applications while running on the tensor cores in the NVIDIA A100 GPU and *Proteus* for narrow data precision input operands (i.e. 4-bit and 8-bit integers). To do so, we (i) identify the subset of our real-world applications that mainly perform GEMM operations and therefore are suitable for the A100's tensor core engines; and (ii) re-implement such workloads using highly optimized instructions to perform tensor GEMM operations on the A100 GPU tensor cores. Re-implementing the GPU workloads is necessary since GPU tensor core instructions are *not* automatically produced via the standard CUDA code our workloads mostly utilize and there is *no* reference implementation available from the original benchmark suites targeting tensor core GPUs. We re-implement three workloads from our real-world applications, i.e., 2mm, 3mm, and gmm, for tensor core execution. To ensure that our re-implemented workloads efficiently utilize the tensor cores, we leverage NVIDIA's open-source CUTLASS library [226], which provides CUDA C++ template abstractions for high-performance GEMM operations and C++ APIs for non-standardized data types (4-bit integers, in our case). During data initialization, we ensure that the input data fits into 4-bit or 8-bit data types, depending on the evaluated configuration. As in §7.1, we capture the execution time of the GPU kernel excluding data initialization/transfer time, and we use the `nvml` API [209] to measure GPU energy consumption. We employ all 432 A100's tensor cores during GPU execution.

Fig. 14 shows the tensor cores, SIMD-DRAM, and *Proteus* performance per  $\text{mm}^2$  (Fig. 14a) and energy efficiency (i.e., performance per Watt in Fig. 14b) for three GEMM-heavy real-world applications using 8-bit (`int8`) and 4-bit (`int4`) data types. Values are normalized to the GPU's tensor cores. We make two observations. First, *Proteus* significantly improves performance per  $\text{mm}^2$  and energy efficiency compared to both baselines across all applications and data types. On average across the three applications, *Proteus* achieves (i)  $20\times/43\times$  and  $8\times/21\times$  the performance per  $\text{mm}^2$  and (ii)  $484\times/767\times$  and  $9.8\times/25\times$  the performance per Watt of the tensor cores and SIMD-DRAM, respectively, using `int8/int4` data types. *Proteus* and SIMD-DRAM are capable of outperforming the tensor cores of the A100 GPU for narrow data precisions since both the throughput and the energy efficiency of bit-serial PUD architectures *increase* quadratically for multiplication operations as the bit-precision *decreases* [142]. As a comparison point, both SIMD-DRAM and *Proteus* fail to outperform the baseline CUDA cores in the A100 GPU for the same three workloads when computing over a higher dynamic range (see §7.5). However, such performance and energy efficiency gaps shift in favor of SIMD-DRAM and *Proteus*, particularly when we move from 8 to 4 bit input operands. Second, we observe that by employing dynamic bit-precision and adaptive arithmetic computation, *Proteus* further improves the performance and energy gains that SIMD-DRAM provides compared to the A100 GPU's tensor cores, even improving performance compared to the tensor cores in cases where SIMD-DRAM fails to do so (i.e., for `gmm`).

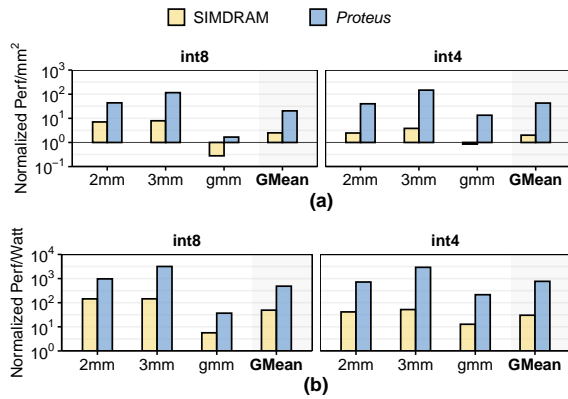


Figure 14: Performance per  $\text{mm}^2$  (a) and performance per Watt (b) of GEMM-intensive real-world applications using `int8` and `int4` data types, normalized to the same metric measured on 432 NVIDIA A100 tensor cores.

## 7.5. Area Analysis

**DRAM Chip Area Overhead.** We use CACTI [188] to evaluate the area overhead of the primary components in the *Proteus* design using a 22 nm technology node. *Proteus* does not introduce any modifications to the DRAM array’s circuitry other than those proposed by (i) *Ambit*, which has an area overhead of  $<1\%$  in a commodity DRAM chip [101]; (ii) *LISA*, which has an area overhead of 0.6% in a commodity DRAM chip [152]; and (iii) *SALP*, which has an area overhead of 0.001% in a commodity DRAM chip [182]. We reserve less than 1 DRAM row (i.e., 6.25 kB in an 8 GB) to store our implemented  $\mu$ Programs. In total, there are 50  $\mu$ Programs, each of which takes 128 B of DRAM space.

**CPU Area Overhead.** We size the *parallelism-aware  $\mu$ Program library* to contain: (i) 16 64 B LUTs, each LUT holding a 8-bit  *$\mu$ Program\_idx*; (ii) one 2 kB  *$\mu$ Program scratchpad* memory. The size of the *parallelism-aware  $\mu$ Program library* is enough to hold one LUT per SIMDRAM PUD operations and address  $2^8$  different  $\mu$ Program implementations. The size of the  *$\mu$ Program scratchpad* is large enough to store the  $\mu$ Programs for all 16 SIMDRAM operations. We use a 128 B scratchpad for the *dynamic bit-precision engine*. We estimate that the *Proteus* control unit area is  $0.03 \text{ mm}^2$ . *Proteus*’s transposition unit (one per DRAM channel) uses an 8 kB fully-associative cache with a 128-bit cache line size for the *object tracker*, and two 4 kB transposition buffers. We estimate the transposition unit area is  $0.06 \text{ mm}^2$ . Considering the area of the control and transposition units, *Proteus* has an area overhead of only 0.03% compared to the die area of an Intel Xeon E5-2697 v3 CPU [113].

## 8. Related Work

To our knowledge, *Proteus* is the first work that provides the hardware support to transparently execute PUD operations with the most bit-precision and arithmetic. We highlight *Proteus*’s key contributions by contrasting them with state-of-the-art PIM designs.

**Processing-Using-DRAM.** Prior works propose different ways of implementing PUD operations [101, 103, 104, 106, 107,

110, 120, 127, 132, 133, 141, 142, 227, 228]. Such works could benefit from *Proteus*’s dynamic bit-precision selection and alternative data representation and algorithms, since they all assume a static bit-precision and algorithmic implementation. AritPIM [199] provides a collection of bit-parallel and bit-serial algorithms for PUM arithmetic. Compared to AritPIM, *Proteus* (i) implements a collection of other bit-parallel algorithms for PUM; (ii) evaluates different data format representations that can lead to further performance and energy improvements; (iii) proposes a framework that can dynamically adapt to the bit-precision of the operation.

**Using Bit-Slicing Compilers & Early Termination for PIM.** Prior works [143, 229] propose bit-slicing compilers for bit-serial PIM computation. In particular, CHOPPER [143] improves SIMDRAM’s programming model by leveraging bit-slicing compilers and employing optimizations to reduce the latency of a  $\mu$ Program. Compared to CHOPPER, *Proteus* has two main advantages. First, *Proteus* improves a  $\mu$ Program performance by *fully* leveraging the DRAM parallelism within a single DRAM bank. Second, although bit-slicing compilers can naturally adapt to different bit-precision values, they require the programmer to specify the target bit-precision manually. In contrast, *Proteus* dynamically identifies the most suitable bit-precision transparently from the programmer. Some other prior works (e.g., [230, 231]) propose techniques to realize early termination of PUM operations for different memory technologies. Compared to these, *Proteus*’s main novelty lies in realizing early termination of bit-serial operation in the context of DRAM/majority-based PUD systems.

## 9. Conclusion

We introduce *Proteus*, an efficient PUD framework with adaptive data precision and dynamic arithmetic. *Proteus* fully leverages the internal parallelism inside a DRAM bank to accelerate the execution of various bit-serial and bit-parallel arithmetic operations and dynamically decides the best-performing bit-precision, data representation format, and algorithmic implementation of a PUD operation. We experimentally demonstrate that *Proteus* provides significant benefits over state-of-the-art CPU, GPU, and PUD systems.

## References

- [1] S. Ghose, A. Boroumand, J. S. Kim, J. Gómez-Luna, and O. Mutlu, “Processing-in-Memory: A Workload-Driven Perspective,” *IBM JRD*, 2019.
- [2] O. Mutlu, S. Ghose, J. Gómez-Luna, and R. Ausavarungnirun, “A Modern Primer on Processing in Memory,” in *Emerging Computing: From Devices to Systems – Looking Beyond Moore and Von Neumann*. Springer, 2021.
- [3] G. F. Oliveira, J. Gómez-Luna, L. Orosa, S. Ghose, N. Vijaykumar, I. Fernandez, M. Sadrosadati, and O. Mutlu, “DAMOV: A New Methodology and Benchmark Suite for Evaluating Data Movement Bottlenecks,” *IEEE Access*, 2021.
- [4] S. Ghose, K. Hsieh, A. Boroumand, R. Ausavarungnirun, and O. Mutlu, “The Processing-in-Memory Paradigm: Mechanisms to Enable Adoption,” in *Beyond-CMOS Technologies for Next Generation Computer Design*, 2019.
- [5] O. Mutlu, S. Ghose, J. Gómez-Luna, and R. Ausavarungnirun, “Processing Data Where It Makes Sense: Enabling In-Memory Computation,” *MicPro*, 2019.
- [6] O. Mutlu, S. Ghose, J. Gómez-Luna, and R. Ausavarungnirun, “Enabling Practical Processing in and Near Memory for Data-Intensive Computing,” in *DAC*, 2019.
- [7] O. Mutlu and L. Subramanian, “Research Problems and Opportunities in Memory Systems,” *SUPERFRI*, 2014.
- [8] O. Mutlu, “Memory Scaling: A Systems Architecture Perspective,” in *IMW*, 2013.

- [9] G. H. Loh, N. Jayasena, M. Oskin, M. Nutter, D. Roberts, M. Meswani, D. P. Zhang, and M. Ignatowski, "A Processing in Memory Taxonomy and a Case for Studying Fixed-Function PIM," in *WoNDP*, 2013.
- [10] R. Balasubramonian, J. Chang, T. Manning *et al.*, "Near-Data Processing: Insights from a MICRO-46 Workshop," *IEEE Micro*, 2014.
- [11] H. S. Stone, "A Logic-in-Memory Computer," *IEEE Trans. Comput.*, 1970.
- [12] A. Saulsbury, F. Pong, and A. Nowatzky, "Missing the Memory Wall: The Case for Processor/Memory Integration," in *ISCA*, 1996.
- [13] A. Farmahini-Farahani, J. H. Ahn, K. Morrow, and N. S. Kim, "NDA: Near-DRAM Acceleration Architecture Leveraging Commodity DRAM Devices and Standard Memory Modules," in *HPCA*, 2015.
- [14] O. O. Babarinsa and S. Idreos, "JAFAR: Near-Data Processing for Databases," in *SIGMOD*, 2015.
- [15] F. Devaux, "The True Processing in Memory Accelerator," in *Hot Chips*, 2019.
- [16] N. M. Ghiasi, J. Park, H. Mustafa, J. Kim, A. Olgun, A. Gollwitzer, D. S. Cali, C. Firtina, H. Mao, N. A. Alseer *et al.*, "GenStore: A High-Performance and Energy-Efficient In-Storage Computing System for Genome Sequence Analysis," in *ASPLOS*, 2022.
- [17] J. Gómez-Luna, I. El Hajj, I. Fernandez, C. Giannoula, G. F. Oliveira, and O. Mutlu, "Benchmarking Memory-Centric Computing Systems: Analysis of Real Processing-in-Memory Hardware," in *CUT*, 2021.
- [18] J. Gómez-Luna, I. E. Hajj, I. Fernández, C. Giannoula, G. F. Oliveira, and O. Mutlu, "Benchmarking a New Paradigm: An Experimental Analysis of a Real Processing-in-Memory Architecture," arXiv:2105.03814 [cs.AR], 2021.
- [19] J. Gómez-Luna, I. El Hajj, I. Fernandez, C. Giannoula, G. F. Oliveira, and O. Mutlu, "Benchmarking a New Paradigm: Experimental Analysis and Characterization of a Real Processing-in-Memory System," *IEEE Access*, 2022.
- [20] C. Giannoula, N. Vijaykumar, N. Papadopoulou, V. Karakostas, I. Fernandez, J. Gómez-Luna, L. Orosa, N. Koziris, G. Goumas, and O. Mutlu, "SynCron: Efficient Synchronization Support for Near-Data-Processing Architectures," in *HPCA*, 2021.
- [21] G. Singh, D. Diamantopoulos, C. Hagleitner, J. Gomez-Luna, S. Stuijk, O. Mutlu, and H. Corporaal, "NERO: A Near High-Bandwidth Memory Stencil Accelerator for Weather Prediction Modeling," in *FPL*, 2020.
- [22] S. Lee, K. Kim, S. Oh, J. Park, G. Hong, D. Ka, K. Hwang, J. Park, K. Kang, J. Kim, J. Jeon, N. Kim, Y. Kwon, K. Vladimirov, W. Shin, J. Won, M. Lee, H. Joo *et al.*, "A 1ynm 1.25V 8Gb, 16Gb/s/pin GDDR6-based Accelerator-in-Memory Supporting 1TFLOPS MAC Operation and Various Activation Functions for Deep-Learning Applications," in *ISSCC*, 2022.
- [23] L. Ke, X. Zhang, J. So, J.-G. Lee, S.-H. Kang, S. Lee, S. Han, Y. Cho, J. H. Kim, Y. Kwon *et al.*, "Near-Memory Processing in Action: Accelerating Personalized Recommendation with AxDIMM," *IEEE Micro*, 2021.
- [24] C. Giannoula, I. Fernandez, J. G. Luna, N. Koziris, G. Goumas, and O. Mutlu, "SparseP: Towards Efficient Sparse Matrix Vector Multiplication on Real Processing-in-Memory Architectures," in *SIGMETRICS*, 2022.
- [25] H. Shin, D. Kim, E. Park, S. Park, Y. Park, and S. Yoo, "McDRAM: Low Latency and Energy-Efficient Matrix Computations in DRAM," *IEEE TCADICS*, 2018.
- [26] S. Cho, H. Choi, E. Park, H. Shin, and S. Yoo, "McDRAM v2: In-Dynamic Random Access Memory Systolic Array Accelerator to Address the Large Model Problem in Deep Neural Networks on the Edge," *IEEE Access*, 2020.
- [27] A. Denzler, R. Bera, N. Hajinazar, G. Singh, G. F. Oliveira, J. Gómez-Luna, and O. Mutlu, "Casper: Accelerating Stencil Computation using Near-Cache Processing," arXiv:2112.14216 [cs.AR], 2021.
- [28] H. Asghari-Moghaddam, Y. H. Son, J. H. Ahn, and N. S. Kim, "Chameleon: Versatile and Practical Near-DRAM Acceleration Architecture for Large Memory Systems," in *MICRO*, 2016.
- [29] D. Patterson, T. Anderson, N. Cardwell *et al.*, "A Case for Intelligent RAM," *IEEE Micro*, 1997.
- [30] D. G. Elliott, M. Stumm, W. M. Snelgrove *et al.*, "Computational RAM: Implementing Processors in Memory," *Design and Test of Computers*, vol. 16, no. 1, pp. 32–41, Jan. 1999.
- [31] M. A. Z. Alves, P. C. Santos, F. B. Moreira, and others, "Saving memory movements through vector processing in the dram," in *Int. Conf. on Compilers, Architecture and Synthesis for Embedded Systems*, 2015.
- [32] S. L. Xi, O. Babarinsa, M. Athanassoulis, and S. Idreos, "Beyond the wall: Near-data processing for databases," in *Int. Workshop on Data Management on New Hardware*, 2015.
- [33] W. Sun, Z. Li, S. Yin, S. Wei, and L. Liu, "ABC-DIMM: Alleviating the Bottleneck of Communication in DIMM-Based Near-Memory Processing with Inter-DIMM Broadcast," in *ISCA*, 2021.
- [34] K. K. Matam, G. Koo, H. Zha, H.-W. Tseng, and M. Annavaram, "GraphSSD: Graph Semantics Aware SSD," in *ISCA*, 2019.
- [35] M. Gokhale, B. Holmes, and K. Jobst, "Processing in Memory: The Terasys Massively Parallel PIM Array," *Computer*, 1995.
- [36] M. Hall, P. Kogge, J. Koller, P. Diniz, J. Chame, J. Draper, J. LaCoss, J. Granacki, J. Brockman, A. Srivastava *et al.*, "Mapping Irregular Applications to DIVA, a PIM-Based Data-Intensive Architecture," in *SC*, 1999.
- [37] M. A. Z. Alves, P. C. Santos, M. Diener, and L. Carro, "Opportunities and Challenges of Performing Vector Operations Inside the DRAM," in *MEMSYS*, 2015.
- [38] E. Lockerman, A. Feldmann, M. Bakhshalipour, A. Stanescu, S. Gupta, D. Sanchez, and N. Beckmann, "Livia: Data-Centric Computing Throughout the Memory Hierarchy," in *ASPLOS*, 2020.
- [39] J. Ahn, S. Hong, S. Yoo, O. Mutlu, and K. Choi, "A Scalable Processing-in-Memory Accelerator for Parallel Graph Processing," in *ISCA*, 2015.
- [40] L. Nai, R. Hadidi, J. Sim, H. Kim, P. Kumar, and H. Kim, "GraphPIM: Enabling Instruction-Level PIM Offloading in Graph Computing Frameworks," in *HPCA*, 2017.
- [41] A. Boroumand, S. Ghose, Y. Kim, R. Ausavarungrinun, E. Shiu, R. Thakur, D. Kim, A. Kuusela, A. Knies, P. Ranganathan *et al.*, "Google Workloads for Consumer Devices: Mitigating Data Movement Bottlenecks," in *ASPLOS*, 2018.
- [42] A. Boroumand, S. Ghose, B. Lucia, K. Hsieh, K. Malladi, H. Zheng, and O. Mutlu, "LazyPIM: An Efficient Cache Coherence Mechanism for Processing-in-Memory," *CAL*, 2017.
- [43] D. Zhang, N. Jayasena, A. Lyashevsky, J. L. Greathouse, L. Xu, and M. Ignatowski, "TOP-PIM: Throughput-Oriented Programmable Processing in Memory," in *HPDC*, 2014.
- [44] M. Gao and C. Kozyrakis, "HRL: Efficient and Flexible Reconfigurable Logic for Near-Data Processing," in *HPCA*, 2016.
- [45] J. S. Kim, D. S. Cali, H. Xin, D. Lee, S. Ghose, M. Alser, H. Hassan, O. Ergin, C. Alkan, and O. Mutlu, "GRIM-Filter: Fast Seed Location Filtering in DNA Read Mapping Using Processing-in-Memory Technologies," *BMC Genomics*, 2018.
- [46] M. Drumond, A. Daglis, N. Mirzadeh, D. Ustiugov, J. Picorel, B. Falsafi, B. Grot, and D. Pneumatikatos, "The Mondrian Data Engine," in *ISCA*, 2017.
- [47] P. C. Santos, G. F. Oliveira, D. G. Tomé, M. A. Z. Alves, E. C. Almeida, and L. Carro, "Operand Size Reconfiguration for Big Data Processing in Memory," in *DATE*, 2017.
- [48] G. F. Oliveira, P. C. Santos, M. A. Alves, and L. Carro, "NIM: An HMC-Based Machine for Neuron Computation," in *ARC*, 2017.
- [49] J. Ahn, S. Yoo, O. Mutlu, and K. Choi, "PIM-Enabled Instructions: A Low-Overhead, Locality-Aware Processing-in-Memory Architecture," in *ISCA*, 2015.
- [50] M. Gao, J. Pu, X. Yang, M. Horowitz, and C. Kozyrakis, "TETRIS: Scalable and Efficient Neural Network Acceleration with 3D Memory," in *ASPLOS*, 2017.
- [51] D. Kim, J. Kung, S. Chai, S. Yalamanchili, and S. Mukhopadhyay, "Neurocube: A Programmable Digital Neuromorphic Architecture with High-Density 3D Memory," in *ISCA*, 2016.
- [52] P. Gu, S. Li, D. Stow, R. Barnes, L. Liu, Y. Xie, and E. Kursun, "Leveraging 3D Technologies for Hardware Security: Opportunities and Challenges," in *GLSVLSI*, 2016.
- [53] A. Boroumand, S. Ghose, M. Patel, H. Hassan, B. Lucia, R. Ausavarungrinun, K. Hsieh, N. Hajinazar, K. T. Malladi, H. Zheng *et al.*, "CoNDA: Efficient Cache Coherence Support for Near-Data Accelerators," in *ISCA*, 2019.
- [54] K. Hsieh, E. Ebrahimi, G. Kim, N. Chatterjee, M. O'Connor, N. Vijaykumar, O. Mutlu, and S. W. Keckler, "Transparent Offloading and Mapping (TOM) Enabling Programmer-Transparent Near-Data Processing in GPU Systems," in *ISCA*, 2016.
- [55] D. S. Cali, G. S. Kalsi, Z. Bingöl, C. Firtina, L. Subramanian, J. S. Kim, R. Ausavarungrinun, M. Alser, J. Gomez-Luna, A. Boroumand *et al.*, "GenASM: A High-Performance, Low-Power Approximate String Matching Acceleration Framework for Genome Sequence Analysis," in *MICRO*, 2020.
- [56] S. H. Pugsley, J. Jestes, H. Zhang, R. Balasubramonian *et al.*, "NDC: Analyzing the Impact of 3D-Stacked Memory+Logic Devices on MapReduce Workloads," in *ISPASS*, 2014.
- [57] A. Pattnaik, X. Tang, A. Jog, O. Kayiran, A. K. Mishra, M. T. Kandemir, O. Mutlu, and C. R. Das, "Scheduling Techniques for GPU Architectures with Processing-in-Memory Capabilities," in *PACT*, 2016.
- [58] B. Akin, F. Franchetti, and J. C. Hoe, "Data Reorganization in Memory Using 3D-Stacked DRAM," in *ISCA*, 2015.
- [59] K. Hsieh, S. Khan, N. Vijaykumar, K. K. Chang, A. Boroumand, S. Ghose, and O. Mutlu, "Accelerating Pointer Chasing in 3D-Stacked Memory: Challenges, Mechanisms, Evaluation," in *ICCD*, 2016.
- [60] J. H. Lee, J. Sim, and H. Kim, "BSSync: Processing Near Memory for Machine Learning Workloads with Bounded Staleness Consistency Models," in *PACT*, 2015.
- [61] A. Boroumand, S. Ghose, B. Akin, R. Narayanaswami, G. F. Oliveira, X. Ma, E. Shiu, and O. Mutlu, "Mitigating Edge Machine Learning Inference Bottlenecks: An Empirical Study on Accelerating Google Edge Models," arXiv:2103.00768 [cs.AR], 2021.
- [62] A. Boroumand, S. Ghose, B. Akin, R. Narayanaswami, G. F. Oliveira, X. Ma, E. Shiu, and O. Mutlu, "Google Neural Network Models for Edge Devices: Analysis and Mitigating Machine Learning Inference Bottlenecks," in *PACT*, 2021.
- [63] A. Boroumand, S. Ghose, G. F. Oliveira, and O. Mutlu, "Polynesia: Enabling High-Performance and Energy-Efficient Hybrid Transactional/Analytical Databases with Hardware/Software Co-Design," in *ICDE*, 2022.
- [64] A. Boroumand, S. Ghose, G. F. Oliveira, and O. Mutlu, "Polynesia: Enabling Effective Hybrid Transactional/Analytical Databases with Specialized Hardware/Software Co-Design," arXiv:2103.00798 [cs.AR], 2021.
- [65] A. Boroumand, "Practical Mechanisms for Reducing Processor-Memory Data Movement in Modern Workloads," Ph.D. dissertation, Carnegie Mellon University, 2020.
- [66] M. Besta, R. Kanakagiri, G. Kwasniewski, R. Ausavarungrinun, J. Beránek, K. Kanellopoulos, K. Janda, Z. Vonarburg-Shmaria, L. Gianinazzi, I. Stefan *et al.*, "SISA: Set-Centric Instruction Set Architecture for Graph Mining on Processing-in-Memory Systems," in *MICRO*, 2021.
- [67] I. Fernandez, R. Quislan, E. Gutiérrez, O. Plata, C. Giannoula, M. Alser, J. Gómez-Luna, and O. Mutlu, "NATSA: A Near-Data Processing Accelerator for Time Series Analysis," in *ICCD*, 2020.
- [68] G. Singh, G. , G. F. Oliveira, S. Corda, S. Stuijk, O. Mutlu, and H. Corporaal, "NAPEL: Near-Memory Computing Application Performance Prediction via Ensemble Learning," in *DAC*, 2019.
- [69] Y.-C. Kwon, S. H. Lee, J. Lee, S.-H. Kwon, J. M. Ryu, J.-P. Son, O. Seongil, H.-S. Yu, H. Lee, S. Y. Kim *et al.*, "A 20nm 6GB Function-in-Memory DRAM, Based on HBM2

- with a 1.2 TFLOPS Programmable Computing Unit using Bank-Level Parallelism, for Machine Learning Applications,” in *ISSCC*, 2021.
- [70] S. Lee, S.-h. Kang, J. Lee, H. Kim, E. Lee, S. Seo, H. Yoon, S. Lee, K. Lim, H. Shin *et al.*, “Hardware Architecture and Software Stack for PIM Based on Commercial DRAM Technology: Industrial Product,” in *ISCA*, 2021.
- [71] D. Niu, S. Li, Y. Wang, W. Han, Z. Zhang, Y. Guan, T. Guan, F. Sun, F. Xue, L. Duan *et al.*, “184QPS/W 64Mb/mm<sup>2</sup> 3D Logic-to-DRAM Hybrid Bonding with Process-Near-Memory Engine for Recommendation System,” in *ISSCC*, 2022.
- [72] Q. Zhu, T. Graf, H. E. Sumbul, L. Pileggi, and F. Franchetti, “Accelerating Sparse Matrix-Matrix Multiplication with 3D-Stacked Logic-in-Memory Hardware,” in *HPEC*, 2013.
- [73] E. Azarkhish, C. Pfister, D. Rossi, I. Loi, and L. Benini, “Logic-Base Interconnect Design for Near Memory Computing in the Smart Memory Cube,” *IEEE VLSI*, 2016.
- [74] E. Azarkhish, D. Rossi, I. Loi, and L. Benini, “Neurostream: Scalable and Energy Efficient Deep Learning with Smart Memory Cubes,” *TPDS*, 2018.
- [75] Q. Guo, N. Alachiotis, B. Akin, F. Sadi, G. Xu, T. M. Low, L. Pileggi, J. C. Hoe, and F. Franchetti, “3D-Stacked Memory-Side Acceleration: Accelerator and System Design,” in *WoNDP*, 2014.
- [76] J. P. C. de Lima, P. C. Santos, M. A. Alves, A. Beck, and L. Carro, “Design Space Exploration for PIM Architectures in 3D-Stacked Memories,” in *CF*, 2018.
- [77] B. Akin, J. C. Hoe, and F. Franchetti, “HAMLtE: Hardware Accelerated Memory Layout Transform within 3D-Stacked DRAM,” in *HPEC*, 2014.
- [78] Y. Huang, L. Zheng, P. Yao, J. Zhao, X. Liao, H. Jin, and J. Xue, “A Heterogeneous PIM Hardware-Software Co-Design for Energy-Efficient Graph Processing,” in *IPDPS*, 2020.
- [79] G. Dai, T. Huang, Y. Chi, J. Zhao, G. Sun, Y. Liu, Y. Wang, Y. Xie, and H. Yang, “GraphH: A Processing-in-Memory Architecture for Large-Scale Graph Processing,” *TCAD*, 2018.
- [80] J. Liu, H. Zhao, M. A. Ogleari, D. Li, and J. Zhao, “Processing-in-Memory for Energy-Efficient Neural Network Training: A Heterogeneous Approach,” in *MICRO*, 2018.
- [81] P.-A. Tsai, C. Chen, and D. Sanchez, “Adaptive Scheduling for Systems with Asymmetric Memory Hierarchies,” in *MICRO*, 2018.
- [82] P. Gu, X. Xie, Y. Ding, G. Chen, W. Zhang, D. Niu, and Y. Xie, “iPIM: Programmable In-Memory Image Processing Accelerator using Near-Bank Architecture,” in *ISCA*, 2020.
- [83] A. Farmahini-Farahani, J. H. Ahn, K. Compton, and N. S. Kim, “DRAMA: An Architecture for Accelerated Processing Near Memory,” *Computer Architecture Letters*, 2014.
- [84] H. Asghari-Moghaddam, A. Farmahini-Farahani, K. Morrow *et al.*, “Near-DRAM Acceleration with Single-ISA Heterogeneous Processing in Standard Memory Modules,” *IEEE Micro*, 2016.
- [85] J. Huang, R. R. Puli, P. Majumder, S. Kim, R. Boyapati, K. H. Yum, and E. J. Kim, “Active-Routing: Compute on the Way for Near-Data Processing,” in *HPCA*, 2019.
- [86] C. D. Kersey, H. Kim, and S. Yalamanchili, “Lightweight SIMT Core Designs for Intelligent 3D Stacked DRAM,” in *MEMSYS*, 2017.
- [87] J. Li, X. Wang, A. Tumeo, B. Williams, J. D. Leidel, and Y. Chen, “PIMS: A Lightweight Processing-in-Memory Accelerator for Stencil Computations,” in *MEMSYS*, 2019.
- [88] J. S. Kim, D. Senol, H. Xin, D. Lee, S. Ghose, M. Alser, H. Hassan, O. Ergin, C. Alkan, and O. Mutlu, “GRIM-Filter: Fast Seed Filtering in Read Mapping using Emerging Memory Technologies,” arXiv:1708.04329 [q-bio.GN], 2017.
- [89] A. Boroumand, S. Ghose, M. Patel, H. Hassan, B. Lucia, N. Hajinazar, K. Hsieh, K. T. Malladi, H. Zheng, and O. Mutlu, “LazyPIM: Efficient Support for Cache Coherence in Processing-in-Memory Architectures,” arXiv:1706.03162 [cs.AR], 2017.
- [90] Y. Zhuo, C. Wang, M. Zhang, R. Wang, D. Niu, Y. Wang, and X. Qian, “GraphQ: Scalable PIM-Based Graph Processing,” in *MICRO*, 2019.
- [91] M. Zhang, Y. Zhuo, C. Wang, M. Gao, Y. Wu, K. Chen, C. Kozyrakis, and X. Qian, “GraphP: Reducing Communication for PIM-Based Graph Processing with Efficient Data Partition,” in *HPCA*, 2018.
- [92] H. Lim and G. Park, “Triple Engine Processor (TEP): A Heterogeneous Near-Memory Processor for Diverse Kernel Operations,” *TACO*, 2017.
- [93] E. Azarkhish, D. Rossi, I. Loi, and L. Benini, “A Case for Near Memory Computation Inside the Smart Memory Cube,” in *EMS*, 2016.
- [94] M. A. Z. Alves, M. Diener, P. C. Santos, and L. Carro, “Large Vector Extensions Inside the HMC,” in *DATE*, 2016.
- [95] J. Jang, J. Heo, Y. Lee, J. Won, S. Kim, S. J. Jung, H. Jang, T. J. Ham, and J. W. Lee, “Charon: Specialized Near-Memory Processing Architecture for Clearing Dead Objects in Memory,” in *MICRO*, 2019.
- [96] R. Nair, S. F. Antao, C. Bertolli, P. Bose *et al.*, “Active Memory Cube: A Processing-in-Memory Architecture for Exascale Systems,” *IBM JRD*, 2015.
- [97] R. Hadidi, L. Nai, H. Kim, and H. Kim, “CAIRO: A Compiler-Assisted Technique for Enabling Instruction-Level Offloading of Processing-in-Memory,” *TACO*, 2017.
- [98] P. C. Santos, G. F. Oliveira, J. P. Lima, M. A. Alves, L. Carro, and A. C. Beck, “Processing in 3D Memories to Speed Up Operations on Complex Data Structures,” in *DATE*, 2018.
- [99] P. Chi, S. Li, C. Xu, T. Zhang, J. Zhao, Y. Liu, Y. Wang, and Y. Xie, “PRIME: A Novel Processing-in-Memory Architecture for Neural Network Computation in ReRAM-Based Main Memory,” in *ISCA*, 2016.
- [100] A. Shafiee, A. Nag, N. Muralimanohar, B. Balasubramanian, J. P. Strachan, M. Hu, R. S. Williams, and V. Srikumar, “ISAAC: A Convolutional Neural Network Accelerator with In-Situ Analog Arithmetic in Crossbars,” in *ISCA*, 2016.
- [101] V. Seshadri, D. Lee, T. Mullins, H. Hassan, A. Boroumand, J. Kim, M. A. Kozuch, O. Mutlu, P. B. Gibbons, and T. C. Mowry, “Ambit: In-Memory Accelerator for Bulk Bitwise Operations Using Commodity DRAM Technology,” in *MICRO*, 2017.
- [102] V. Seshadri and O. Mutlu, “In-DRAM Bulk Bitwise Execution Engine,” arXiv:1905.09822 [cs.AR], 2019.
- [103] S. Li, D. Niu, K. T. Malladi, H. Zheng, B. Brennan, and Y. Xie, “DRISA: A DRAM-Based Reconfigurable In-Situ Accelerator,” in *MICRO*, 2017.
- [104] V. Seshadri, Y. Kim, C. Fallin, D. Lee, R. Ausavarungnirun, G. Pekhimenko, Y. Luo, O. Mutlu, P. B. Gibbons, M. A. Kozuch *et al.*, “RowClone: Fast and Energy-Efficient In-DRAM Bulk Data Copy and Initialization,” in *MICRO*, 2013.
- [105] V. Seshadri and O. Mutlu, “The Processing Using Memory Paradigm: In-DRAM Bulk Copy, Initialization, Bitwise AND and OR,” arXiv:1610.09603 [cs.AR], 2016.
- [106] Q. Deng, L. Jiang, Y. Zhang, M. Zhang, and J. Yang, “DrAcc: A DRAM Based Accelerator for Accurate CNN Inference,” in *DAC*, 2018.
- [107] X. Xin, Y. Zhang, and J. Yang, “ELP2IM: Efficient and Low Power Bitwise Operation Processing in DRAM,” in *HPCA*, 2020.
- [108] L. Song, Y. Zhuo, X. Qian, H. Li, and Y. Chen, “GraphR: Accelerating Graph Processing Using ReRAM,” in *HPCA*, 2018.
- [109] L. Song, X. Qian, H. Li, and Y. Chen, “PipeLayer: A Pipelined ReRAM-Based Accelerator for Deep Learning,” in *HPCA*, 2017.
- [110] F. Gao, G. Tziantzioulis, and D. Wentzloff, “ComputeDRAM: In-Memory Compute Using Off-the-Shelf DRAMs,” in *MICRO*, 2019.
- [111] C. Eckert, X. Wang, J. Wang, A. Subramanian, R. Iyer, D. Sylvester, D. Blaauw, and R. Das, “Neural Cache: Bit-Serial In-Cache Acceleration of Deep Neural Networks,” in *ISCA*, 2018.
- [112] S. Aga, S. Jeloka, A. Subramanian, S. Narayanasamy, D. Blaauw, and R. Das, “Compute Caches,” in *HPCA*, 2017.
- [113] D. Fujiki, S. Mahlke, and R. Das, “Duality Cache for Data Parallel Acceleration,” in *ISCA*, 2019.
- [114] V. Seshadri, D. Lee, T. Mullins, H. Hassan, A. Boroumand, J. Kim, M. A. Kozuch, O. Mutlu, P. B. Gibbons, and T. C. Mowry, “Buddy-RAM: Improving the Performance and Efficiency of Bulk Bitwise Operations Using DRAM,” arXiv:1611.09988 [cs.AR], 2016.
- [115] V. Seshadri and O. Mutlu, “Simple Operations in Memory to Reduce Data Movement,” in *Advances in Computers, Volume 106*, 2017.
- [116] V. Seshadri, Y. Kim, C. Fallin, D. Lee, R. Ausavarungnirun, G. Pekhimenko, Y. Luo, O. Mutlu, P. B. Gibbons, M. A. Kozuch *et al.*, “RowClone: Accelerating Data Movement and Initialization Using DRAM,” arXiv:1805.03502 [cs.AR], 2018.
- [117] V. Seshadri, K. Hsieh, A. Boroumand, D. Lee, M. A. Kozuch, O. Mutlu, P. B. Gibbons, and T. C. Mowry, “Fast Bulk Bitwise AND and OR in DRAM,” *CAL*, 2015.
- [118] S. Li, C. Xu, J. Zhao, Y. Lu, and Y. Xie, “Pinatubo: A Processing-in-Memory Architecture for Bulk Bitwise Operations in Emerging Non-Volatile Memories,” in *DAC*, 2016.
- [119] J. D. Ferreira, G. Falcao, J. Gómez-Luna, M. Alser, L. Orosa, M. Sadrosadati, J. S. Kim, G. F. Oliveira, T. Shahroodi, A. Nori *et al.*, “pLUTo: In-DRAM Lookup Tables to Enable Massively Parallel General-Purpose Computation,” arXiv:2104.07699 [cs.AR], 2021.
- [120] J. D. Ferreira, G. Falcao, J. Gómez-Luna, M. Alser, L. Orosa, M. Sadrosadati, J. S. Kim, G. F. Oliveira, T. Shahroodi, A. Nori *et al.*, “pLUTo: Enabling Massively Parallel Computation in DRAM via Lookup Tables,” in *MICRO*, 2022.
- [121] M. Imani, S. Gupta, Y. Kim, and T. Rosing, “FloatPIM: In-Memory Acceleration of Deep Neural Network Training with High Precision,” in *ISCA*, 2019.
- [122] Z. He, L. Yang, S. Angizi, A. S. Rakin, and D. Fan, “Sparse BD-Net: A Multiplication-Less DNN with Sparse Binarized Depth-Wise Separable Convolution,” *JETC*, 2020.
- [123] J. Park, R. Azizi, G. F. Oliveira, M. Sadrosadati, R. Nadig, D. Novo, J. Gómez-Luna, M. Kim, and O. Mutlu, “Flash-Cosmos: In-Flash Bulk Bitwise Operations Using Inherent Computation Capability of NAND Flash Memory,” in *MICRO*, 2022.
- [124] M. S. Truong, L. Shen, A. Glass, A. Hoffmann, L. R. Carley, J. A. Bain, and S. Ghose, “Adapting the RACER Architecture to Integrate Improved In-ReRAM Logic Primitives,” *JTCAS*, 2022.
- [125] M. S. Truong, E. Chen, D. Su, L. Shen, A. Glass, L. R. Carley, J. A. Bain, and S. Ghose, “RACER: Bit-Pipelined Processing Using Resistive Memory,” in *MICRO*, 2021.
- [126] A. Olgun, M. Patel, A. G. Yağlıkçı, H. Luo, J. S. Kim, F. N. Bostancı, N. Vijaykumar, O. Ergin, and O. Mutlu, “QUAC-TRNG: High-Throughput True Random Number Generation Using Quadruple Row Activation in Commodity DRAMs,” in *ISCA*, 2021.
- [127] J. S. Kim, M. Patel, H. Hassan, L. Orosa, and O. Mutlu, “D-RaNGe: Using Commodity DRAM Devices to Generate True Random Numbers With Low Latency and High Throughput,” in *HPCA*, 2019.
- [128] J. S. Kim, M. Patel, H. Hassan, and O. Mutlu, “The DRAM Latency PUF: Quickly Evaluating Physical Unclonable Functions by Exploiting the Latency-Reliability Tradeoff in Modern Commodity DRAM Devices,” in *HPCA*, 2018.
- [129] F. N. Bostancı, A. Olgun, L. Orosa, A. G. Yağlıkçı, J. S. Kim, H. Hassan, O. Ergin, and O. Mutlu, “DR-STaNGe: End-to-End System Design for DRAM-Based True Random Number Generators,” in *HPCA*, 2022.
- [130] A. Olgun, J. G. Luna, K. Kanellopoulos, B. Salami, H. Hassan, O. Ergin, and O. Mutlu, “PiDRAM: A Holistic End-to-End FPGA-Based Framework for Processing-in-DRAM,” *TACO*, 2022.
- [131] M. F. Ali, A. Jaiswal, and K. Roy, “In-Memory Low-Cost Bit-Serial Addition Using Commodity DRAM Technology,” in *TCAS-I*, 2019.
- [132] S. Angizi and D. Fan, “GraphiDe: A Graph Processing Accelerator Leveraging In-DRAM-Computing,” in *GLSVLSI*, 2019.
- [133] S. Li, A. O. Glova, X. Hu, P. Gu, D. Niu, K. T. Malladi, H. Zheng, B. Brennan, and Y. Xie, “SCOPE: A Stochastic Computing Engine for DRAM-Based In-Situ Accelerator,” in *MICRO*, 2018.
- [134] A. Subramanian and R. Das, “Parallel Automata Processor,” in *ISCA*, 2017.

- [135] Y. Zha and J. Li, "Hyper-AP: Enhancing Associative Processing Through A Full-Stack Optimization," in *ISCA*, 2020.
- [136] D. Fujiki, S. Mahlke, and R. Das, "In-Memory Data Parallel Processor," in *ASPLOS*, 2018.
- [137] L. Orosa, Y. Wang, M. Sadrosadati, J. Kim, M. Patel, I. Puddu, H. Luo, K. Razavi, J. Gómez-Luna, H. Hassan, N. M. Ghiasi, S. Ghose, and O. Mutlu, "CODIC: A Low-Cost Substrate for Enabling Custom In-DRAM Functionalities and Optimizations," in *ISCA*, 2021.
- [138] M. Sharad, D. Fan, and K. Roy, "Ultra Low Power Associative Computing with Spin Neurons and Resistive Crossbar Memory," in *DAC*, 2013.
- [139] S. H. S. Rezaei, M. Modarressi, R. Ausavarungnirun, M. Sadrosadati, O. Mutlu, and M. Daneshmand, "NoM: Network-on-Memory for Inter-Bank Data Transfer in Highly-Banked Memories," *CAL*, 2020.
- [140] I. E. Yuksel, Y. C. Tuğrul, A. Olgun, F. N. Bostanci, A. G. Yaglikçi, G. F. Oliveira, H. Luo, J. Gómez-Luna, M. Sadrosadati, and O. Mutlu, "Functionally-Complete Boolean Logic in Real DRAM Chips: Experimental Characterization and Analysis," in *HPCA*, 2024.
- [141] G. F. Oliveira, A. Olgun, A. G. G. Yaglikçi, N. Bostanci, J. Gómez-Luna, S. Ghose, and O. Mutlu, "MIMDRAM: An End-to-End Processing-Using-DRAM System for High-Throughput, Energy-Efficient and Programmer-Transparent Multiple-Instruction Multiple-Data Computing," in *HPCA*, 2024.
- [142] N. Hajinazar, G. F. Oliveira, S. Gregorio, J. D. Ferreira, N. M. Ghiasi, M. Patel, M. Alser, S. Ghose, J. Gómez-Luna, and O. Mutlu, "SIMDRAM: A Framework for Bit-Serial SIMD Processing Using DRAM," in *ASPLOS*, 2021.
- [143] X. Peng, Y. Wang, and M.-C. Yang, "CHOPPER: A Compiler Infrastructure for Programmable Bit-Serial SIMD Processing Using Memory In DRAM," in *HPCA*, 2023.
- [144] C. Guest and T. K. Gaylord, "Truth-Table Look-Up Optical Processing Utilizing Binary and Residue Arithmetic," *Applied Optics*, 1980.
- [145] D. S. Phatak and I. Koren, "Hybrid Signed-Digit Number Systems: A Unified Framework for Redundant Number Representations with Bounded Carry Propagation Chains," *TC*, 1994.
- [146] M. Lapointe, H. T. Huynh, and P. Fortier, "Systematic Design of Pipelined Recursive Filters," *TC*, 1993.
- [147] J. Kim, M. Patel, H. Hassan, and O. Mutlu, "Solar-DRAM: Reducing DRAM Access Latency by Exploiting the Variation in Local Bitlines," in *ICCD*, 2018.
- [148] D. Lee, S. Khan, L. Subramanian, S. Ghose, R. Ausavarungnirun, G. Pekhimenko, V. Seshadri, and O. Mutlu, "Design-Induced Latency Variation in Modern DRAM Chips: Characterization, Analysis, and Latency Reduction Mechanisms," in *SIGMETRICS*, 2017.
- [149] C. Kim, D. Burger, and S. W. Keckler, "An Adaptive, Non-Uniform Cache Structure for Wire-Delay Dominated On-Chip Caches," in *ASPLOS*, 2002.
- [150] K.-N. Lim, W.-J. Jang, H.-S. Won, K.-Y. Lee, H. Kim, D.-W. Kim, M.-H. Cho, S.-L. Kim, J.-H. Kang, K.-W. Park *et al.*, "A 1.2 V 23nm 6F2 4Gb DDR3 SDRAM with Local-Bitline Sense Amplifier, Hybrid LIO Sense Amplifier and Dummy-Less Array Architecture," in *ISSCC*, 2012.
- [151] T. Takahashi, T. Sekiguchi, R. Takemura, S. Narui, H. Fujisawa, S. Miyatake, M. Morino, K. Arai, S. Yamada, S. Shukuri *et al.*, "A Multigigabit DRAM Technology with 6F2 Open-Bitline Cell, Distributed Overdriven Sensing, and Stacked-Flash Fuse," *JSSC*, 2001.
- [152] K. K. Chang, P. J. Nair, D. Lee, S. Ghose, M. K. Qureshi, and O. Mutlu, "Low-Cost Inter-Linked Subarrays (LISA): Enabling Fast Inter-Subarray Data Movement in DRAM," in *HPCA*, 2016.
- [153] G. Pekhimenko, V. Seshadri, O. Mutlu, M. A. Kozuch, P. B. Gibbons, and T. C. Mowry, "Base-Delta-Immediate Compression: Practical Data Compression for On-Chip Caches," in *PACT*, 2012.
- [154] A. R. Alameldeen and D. A. Wood, "Adaptive Cache Compression for High-Performance Processors," in *ISCA*, 2004.
- [155] M. M. Islam and P. Stenstrom, "Characterization and Exploitation of Narrow-Width Loads: The Narrow-Width Cache Approach," in *CASES*, 2010.
- [156] O. Ergin, O. Unsal, X. Vera, and A. Gonzalez, "Exploiting Narrow Values for Soft Error Tolerance," *Comp. Arch. Lett.*, 2006.
- [157] D. Brooks and M. Martonosi, "Dynamically Exploiting Narrow Width Operands to Improve Processor Power and Performance," in *HPCA*, 1999.
- [158] O. Ergin, D. Balkan, K. Ghose, and D. Ponomarev, "Register Packing: Exploiting Narrow-Width Operands for Reducing Register File Pressure," in *MICRO*, 2004.
- [159] M. Budiu, M. Sakr, K. Walker, and S. C. Goldstein, "BitValue Inference: Detecting and Exploiting Narrow Bitwidth Computations," in *Euro-Par*, 2000.
- [160] P. R. Wilson, S. F. Kaplan, and Y. Smaragdakis, "The Case for Compressed Caching in Virtual Memory Systems," in *USENIX ATC*, 1999.
- [161] X. Wang and W. Zhang, "GPU Register Packing: Dynamically Exploiting Narrow-Width Operands to Improve Performance," in *TrustCom*, 2017.
- [162] J. Hu, S. Wang, and S. G. Ziavras, "In-Register Duplication: Exploiting Narrow-Width Value for Improving Register File Reliability," in *DSN*, 2006.
- [163] S. Wang, J. Hu, S. G. Ziavras, and S. W. Chung, "Exploiting Narrow-Width Values for Thermal-Aware Register File Designs," in *DATE*, 2009.
- [164] M. Canesche, R. Ferreira, J. A. Nacif, and F. M. Quintão Pereira, "A Polynomial Time Exact Solution to the Bit-Aware Register Binding Problem," in *CC*, 2022.
- [165] A. Canis, J. Choi, B. Fort, R. Lian, Q. Huang, N. Calagar, M. Gort, J. J. Qin, M. Aldham, T. Czajkowski *et al.*, "From Software to Accelerators with LegUp High-Level Synthesis," in *CASES*, 2013.
- [166] C. Pilato and F. Ferrandi, "Bambu: A Modular Framework for the High Level Synthesis of Memory-Intensive Applications," in *FPL*, 2013.
- [167] C. Lattner, "LLVM and Clang: Next Generation Compiler Technology," in *BSDCan*, 2008.
- [168] S. Sarda and M. Pandey, *LLVM Essentials*. Packt Publishing Ltd, 2015.
- [169] B. C. Lopes and R. Auler, *Getting Started with LLVM Core Libraries*. Packt Publishing Ltd, 2014.
- [170] A. Sampson, "LLVM for Grad Students," <https://www.cs.cornell.edu/~asampson/blog/llvm.html>.
- [171] M. H. Lipasti, B. R. Mestan, and E. Gunadi, "Physical Register Inlining," in *ISCA*, 2004.
- [172] G. H. Loh, "Exploiting Data-Width Locality to Increase Superscalar Execution Bandwidth," in *MICRO*, 2002.
- [173] M. Stephenson, J. Babb, and S. Amarasinghe, "Bitwidth Analysis with Application to Silicon Compilation," in *PLDI*, 2000.
- [174] R. E. Rodrigues, V. H. S. Campos, and F. M. Q. Pereira, "A Fast and Low-Overhead Technique to Secure Programs Against Integer Overflows," in *CGO*, 2013.
- [175] V. H. S. Campos, R. E. Rodrigues, I. R. de Assis Costa, and F. M. Q. Pereira, "Speed and Precision in Range Analysis," in *SBLP*, 2012.
- [176] J. Cong, Y. Fan, G. Han, Y. Lin, J. Xu, Z. Zhang, and X. Cheng, "Bitwidth-Aware Scheduling and Binding in High-level Synthesis," in *ASP-DAC*, 2005.
- [177] J. Olivares, J. Hormigo, J. Villalba, I. Benavides, and E. L. Zapata, "SAD Computation based on Online Arithmetic for Motion Estimation," *Microprocessors and Microsystems*, 2006.
- [178] J. Olivares, J. Hormigo, J. Villalba, and I. Benavides, "Minimum Sum of Absolute Differences Implementation in a Single FPGA Device," in *FPL*, 2004.
- [179] M. D. Brown and Y. N. Patt, "Using Internal Redundant Representations and Limited Bypass to Support Pipelined Adders and Register Files," in *HPCA*, 2002.
- [180] Intel Corp., *Intel® 64 and IA-32 Architectures Software Developer's Manual, Vol. 3*, 2016.
- [181] UPMEM, "UPMEM Website," <https://www.upmem.com>, 2020.
- [182] Y. Kim, V. Seshadri, D. Lee, J. Liu, and O. Mutlu, "A Case for Exploiting Subarray-Level Parallelism (SALP) in DRAM," in *ISCA*, 2012.
- [183] O. J. Bedrij, "Carry-Select Adder," *IEEE Trans. Comput.*, 1962.
- [184] P. M. Kogge and H. S. Stone, "A Parallel Algorithm for the Efficient Solution of a General Class of Recurrence Equations," *IEEE Trans. Comput.*, 1973.
- [185] R. E. Ladner and M. J. Fischer, "Parallel Prefix Computation," *JACM*, 1980.
- [186] Brent and Kung, "A Regular Layout for Parallel Adders," *IEEE Transactions on Computers*, 1982.
- [187] H. Makino, Y. Nakase, H. Suzuki, H. Morinaka, H. Shinohara, and K. Mashiko, "An 8.8-ns 54/SPL Times/54-bit Multiplier with High Speed Redundant Binary Architecture," *JSSC*, 1996.
- [188] P. Shivakumar and N. P. Jouppi, "CACTI 3.0: An Integrated Cache Timing, Power, and Area Model," Compaq Computer Corporation, Tech. Rep. 2001/2, 2001.
- [189] A. A. Karatsuba and Y. P. Ofman, "Multiplication of Many-Digital Numbers by Automatic Computers," in *USSR Academy of Sciences*, 1962.
- [190] I. Goodfellow, Y. Bengio, and A. Courville, *Deep Learning*. MIT Press, 2016.
- [191] S. Han, X. Liu, H. Mao, J. Pu, A. Pedram, M. A. Horowitz, and W. J. Dally, "EIE: Efficient Inference Engine on Compressed Deep Neural Network," in *ISCA*, 2016.
- [192] SAFARI Research Group, "DAMOV Benchmark Suite and Simulation Framework," <https://github.com/CMU-SAFARI/DAMOV>.
- [193] N. Muralimanohar, R. Balasubramanian, and N. Jouppi, "Optimizing NUCA Organizations and Wiring Alternatives for Large Caches with CACTI 6.0," in *MICRO*, 2007.
- [194] JEDEC, "DDR3 SDRAM Standard," *JEDEC Standard*, no. 79-3F, 2012.
- [195] JEDEC, "JEDEC Standard: DDR4 SDRAM," *JESD79-4*, Sep, 2012.
- [196] JEDEC, "JEDEC Standard: DDR4 SDRAM," *JESD79-4C*, June, 2012.
- [197] Micron, "Micron Collaborates with Broadcom to Solve DRAM Timing Challenge, Delivering Improved Performance for Networking Customers," <https://bit.ly/3Rmx10L>, 2013.
- [198] M. He, C. Song, I. Kim, C. Jeong, S. Kim, I. Park, M. Thottethodi, and T. Vijaykumar, "Newton: A DRAM-Maker's Accelerator-in-Memory (AiM) Architecture for Machine Learning," in *MICRO*, 2020.
- [199] O. Leitersdorf, D. Leitersdorf, J. Gal, M. Dahan, R. Ronen, and S. Kvatinsky, "AritPIM: High-Throughput In-Memory Arithmetic," *IEEE Trans. Emerg. Topics Comput.*, 2023.
- [200] Y. Onur Koçberber, Y. Osmanlioğlu, and O. Ergin, "Exploiting Narrow Values for Faster Parity Generation," *Microelectronics International*, 2009.
- [201] IEEE Computer Society, "IEEE 754-2008: IEEE Standard for Floating-Point Arithmetic," 2008.
- [202] Intel Corp., "6th Generation Intel Core Processor Family Datasheet," <http://www.intel.com/content/www/us/en/processors/core/>.
- [203] NVIDIA, "NVIDIA A100 Tensor Core GPU Architecture. White Paper," <https://images.nvidia.com/aem-dam/en-zz/Solutions/data-center/nvidia-ampere-architecture-whitepaper.pdf>, 2020.
- [204] N. Firasta, M. Buxton, P. Jinbo, K. Nasri, and S. Kuo, "Intel AVX: New Frontiers in Performance Improvements and Energy Efficiency," Intel Corp., 2008, white paper.
- [205] N. Binkert, B. Beckmann, G. Black, S. K. Reinhardt, A. Saidi, A. Basu, J. Hestness, D. R. Hower, T. Krishna, S. Sardashti, R. Sen, K. Sewell, M. Shoab, M. D. Hill, and D. A. Wood, "The gem5 Simulator," *Comput. Archit. News*, 2011.
- [206] SAFARI Research Group, "MIMDRAM Simulation Framework," <https://github.com/CMU-SAFARI/MIMDRAM>.
- [207] H. Hassan, A. Olgun, A. G. Yaglikçi, H. Luo, and O. Mutlu, "A Case for Self-Managing DRAM Chips: Improving Performance, Efficiency, Reliability, and Security via Autonomous in-DRAM Maintenance Operations," arXiv:2207.13358 [cs.AR], 2022.
- [208] M. Hähnle, B. Döbel, M. Völp, and H. Härtig, "Measuring Energy Consumption for Short Code Paths Using RAPL," *SIGMETRICS*, 2012.



- [209] NVIDIA Corp., “NVIDIA Management Library (NVML),” <https://developer.nvidia.com/nvidia-management-library-nvml>.
- [210] Intel Corp., “10th Generation Intel Core Processor Family Datasheet,” <https://www.intel.com/content/www/us/en/products/platforms/details/comet-lake-s.html>.
- [211] D. U. Lee, K. W. Kim, K. W. Kim, H. Kim, J. Y. Kim, Y. J. Park, J. H. Kim, D. S. Kim, H. B. Park, J. W. Shin *et al.*, “A 1.2V 8Gb 8-Channel 128GB/s High-Bandwidth Memory (HBM) Stacked DRAM with Effective Microbump I/O Test Methods Using 29nm Process and TSV,” in *ISSCC*, 2014.
- [212] D. Lee, S. Ghose, G. Pekhimenko, S. Khan, and O. Mutlu, “Simultaneous Multi-Layer Access: Improving 3D-Stacked Memory Bandwidth at Low Cost,” *TACO*, 2016.
- [213] O. Mutlu and T. Moscibroda, “Stall-Time Fair Memory Access Scheduling for Chip Multiprocessors,” in *MICRO*, 2007.
- [214] W. K. Zuravleff and T. Robinson, “Controller for a Synchronous DRAM That Maximizes Throughput by Allowing Memory Requests and Commands to Be Issued Out of Order,” U.S. Patent 5 630 096, 1997.
- [215] L.-N. Pouchet, “PolyBench: The Polyhedral Benchmark Suite,” <https://www.cs.colostate.edu/~pouchet/software/polybench/>.
- [216] R. M. Yoo, A. Romano, and C. Kozyrakis, “Phoenix Rebirth: Scalable MapReduce on a Large-Scale Shared-Memory System,” in *IISWC*, 2009.
- [217] S. Che, M. Boyer, J. Meng, D. Tarjan, J. W. Sheaffer, S. Lee, and K. Skadron, “Rodinia: A Benchmark Suite for Heterogeneous Computing,” in *IISWC*, 2009.
- [218] Standard Performance Evaluation Corp., “SPEC CPU2017 Benchmarks,” <http://www.spec.org/cpu2017/>.
- [219] Standard Performance Evaluation Corp., “SPEC CPU2006 Benchmarks,” <http://www.spec.org/cpu2006/>.
- [220] J. A. Stratton, C. Rodrigues, I.-J. Sung, N. Obeid, L.-W. Chang, N. Anssari, G. D. Liu, and W.-m. W. Hwu, “Parboil: A Revised Benchmark Suite for Scientific and Commercial Throughput Computing,” Univ. of Illinois at Urbana-Champaign, IMPACT Research Group, Tech. Rep. IMPACT-12-01, 2012.
- [221] S. C. Woo, M. Ohara, E. Torrie, J. P. Singh, and A. Gupta, “The SPLASH-2 Programs: Characterization and Methodological Considerations,” in *ISCA*, 1995.
- [222] A. Yazdanbakhsh, D. Mahajan, H. Esmailzadeh, and P. Lotfi-Kamran, “AxBench: A Multipatform Benchmark Suite for Approximate Computing,” *IEEE Design & Test*, 2016.
- [223] N.-M. Ho, E. Manogaran, W.-F. Wong, and A. Anooosheh, “Efficient Floating Point Precision Tuning for Approximate Computing,” in *ASP-DAC*, 2017.
- [224] H. Lee, M. Kim, D. Min, J. Kim, J. Back, H. Yoo, J.-H. Lee, and J. Kim, “3D-FPIM: An Extreme Energy-Efficient DNN Acceleration System Using 3D NAND Flash-Based In-Situ PIM Unit,” in *MICRO*, 2022.
- [225] R. Zhou, S. Tabrizchi, M. Morsali, A. Roohi, and S. Angizi, “P-PIM: A Parallel Processing-in-DRAM Framework Enabling Row Hammer Protection,” in *DATE*, 2023.
- [226] NVIDIA Corp., “NVIDIA/cutlass: CUDA Templates for Linear Algebra Subroutines,” <https://github.com/NVIDIA/cutlass>.
- [227] Q. Deng, Y. Zhang, M. Zhang, and J. Yang, “LAcc: Exploiting Lookup Table-Based Fast and Accurate Vector Multiplication in DRAM-Based CNN Accelerator,” in *DAC*, 2019.
- [228] R. Zhou, A. Roohi, D. Misra, and S. Angizi, “FlexiDRAM: A Flexible In-DRAM Framework to Enable Parallel General-Purpose Computation,” in *ISLPED*, 2022.
- [229] A. Arora, A. Bhamburkar, A. Borda, T. Anand, R. Sehgal, B. Hanindhito, P.-E. Gaillardon, J. Kulkarni, and L. K. John, “CoMeFa: Deploying Compute-in-Memory on FPGAs for Deep Learning Acceleration,” *Trans. Reconfigurable Technol. Syst.*, 2023.
- [230] H. Caminal, Y. Chronis, T. Wu, J. M. Patel, and J. F. Martínez, “Accelerating Database Analytic Query Workloads Using an Associative Processor,” in *ISCA*, 2022.
- [231] S. S. Wong, C. C. Tamarit, and J. F. Martínez, “PUMICE: Processing-using-Memory Integration with a Scalar Pipeline for Symbiotic Execution,” in *DAC*, 2023.